



Article

Control and Dynamic Characteristics Analysis for the Double-Compound Axial Piston Pump Based on Working Conditions

Zhiyuan Sun ¹, Qingliang Zeng ^{1,2,*}, Lirong Wan ¹ and Hanzheng Dai ¹

- ¹ College of Mechanical and Electronic Engineering, Shandong University of Science and Technology, Qingdao 266590, China; zysun@sdust.edu.cn (Z.S.); lirong.wan@sdust.edu.cn (L.W.); dhz@tsu.edu.cn (H.D.)
- ² College of Information Science and Engineering, Shandong Normal University, Jinan 250358, China
- * Correspondence: qlzeng@sdust.edu.cn

Abstract: The periodic flow and pressure pulsation of the axial piston pump can lead to periodic vibration, noise, and even damage to various components in the hydraulic system. Therefore, the dynamic characteristics analysis of the axial piston pump in the hydraulic system is of great significance for reducing vibration and noise in the hydraulic system and improving efficiency. The double-compound axial piston pump is the key component of a high power and large flow hydraulic power system, which has a special power control mode. In this paper, the working and control principles of the double-compound axial piston pump are analyzed, the numerical model of the double-compound axial piston pump is established, and the effectiveness of the model is verified through experimental tests. The constant power control characteristics of the double-compound axial piston pump under different power settings and the variable power control characteristics under the rated load pressure are analyzed. By analyzing the dynamic characteristics of the double-compound axial piston pump, the influence of different working conditions on the dynamic characteristics is investigated. The results show that the output efficiency of the double-compound axial piston pump is higher when the output flow is larger. When the piston chamber works in the closed pre-compression pressure zone and the closed pre-release pressure zone, oil backflow occurs. The oil backflow in the piston chamber seriously intensifies the outlet flow pulsation of the double-compound axial piston pump. The flow pulsation rate is positively correlated with load pressure and power control pilot pressure, while negatively correlated with spindle speed. The paper provides a basis for the analysis and optimization of power control, flow pulsation, fluid vibration, and noise of the double-compound axial piston pump.

Keywords: double-compound axial piston pump; power control; dynamic characteristics; flow pulsation; oil backflow



Citation: Sun, Z.; Zeng, Q.; Wan, L.; Dai, H. Control and Dynamic Characteristics Analysis for the Double-Compound Axial Piston Pump Based on Working Conditions. *Machines* **2022**, *10*, 411. <https://doi.org/10.3390/machines10060411>

Academic Editors: Menghua Zhang and Ning Sun

Received: 29 April 2022

Accepted: 23 May 2022

Published: 25 May 2022

Publisher's Note: MDPI stays neutral with regard to jurisdictional claims in published maps and institutional affiliations.



Copyright: © 2022 by the authors. Licensee MDPI, Basel, Switzerland. This article is an open access article distributed under the terms and conditions of the Creative Commons Attribution (CC BY) license (<https://creativecommons.org/licenses/by/4.0/>).

1. Introduction

As a common power transmission mode, hydraulic transmission is more compact, reliable, and controllable than electric and mechanical transmission [1,2]. Therefore, the hydraulic power system is widely used in engineering machinery, transportation, aerospace, and other fields. The axial piston pump is the main power source of the hydraulic system. Because of its structural characteristics, the axial piston pump becomes the main noise source of the hydraulic system [3–5]. Adverse vibration and noise not only affect the stability of the hydraulic system, but also affect the mental state and physiological function of the operator, and even lead to human diseases [6,7]. The noise of the axial piston pump is mainly divided into fluid noise and structural noise. When the low-pressure oil in the piston chamber is pressed into the high-pressure oil discharge chamber, it can be instantly compressed. The oil in the oil discharge chamber instantaneously flows back to the piston

chamber, which is called oil backflow or hydraulic return stroke, forming the oil hammer, which leads to the destruction of uniformity in the oil discharge flow waveform of the piston pump. Similarly, the piston chamber on the barrel block discharges oil, enters the dead zone, and the high-pressure oil in the dead volume cannot be discharged. The piston chamber is instantly connected to the low-pressure oil suction chamber, and the high-pressure oil in the dead volume expands instantaneously, resulting in oil hammer to the oil suction chamber. Excessive flow pulsation can weaken the performance and service life of the pump. Due to the periodic connection of piston chambers with oil suction and discharge chambers, the pressure step is formed, and even positive and negative pressure overshoot occurs, which leads to aeration and cavitation. Flow pulsation, oil backflow, aeration, and cavitation can cause vibration and fluid noise [8]. Structural noise is mainly caused by collision and friction between parts.

The piston is pressed on the swash plate by the slipper retainer through the slipper. As the piston rotates with the barrel block and the swash plate tilts relative to the barrel block shaft, the piston reciprocates in their respective piston chambers. On the other side of the barrel block opposite to the swash plate, a port plate is installed, which is provided with an inlet main groove, an outlet main groove, and a damping structure. The volume of each piston chamber expands and compresses alternately, and the duration of each process is slightly less than half of the spindle rotation period, and there is a short conversion process between the two processes, so that the opening groove of the piston chamber can be connected from one main groove of port plate to another. During the volume expansion of the piston chamber, the hydraulic oil is sucked from the tank through the inlet main groove of the port plate. The squeezing action causes hydraulic oil to be transmitted to the load oil circuit with load pressure through the outlet main groove. Since the processes of the oil suction and oil discharge in the piston chamber are discrete, the flow and pressure at the outlet of the piston pump fluctuate around the average value. These fluctuations are usually called flow pulsation and pressure pulsation, which cause adverse vibration and noise. This periodic flow and pressure pulsation can lead to periodic vibration, noise and even damage of various components in the hydraulic system. Therefore, the dynamic stability of flow and pressure of the double-compound axial piston pump, which is the main power source of construction machinery, directly affects the working stability of the hydraulic system.

In recent years, international scholars have carried out a lot of theoretical, simulation, and experimental research on the flow pulsation and pressure pulsation of the axial piston pump. Edge et al. [9] established an axial piston pump model which considered the influence of oil momentum in the port plate region, and analyzed the influence of the port plate and the damping groove structure on the pressure and flow pulsation of the piston chamber. Manring et al. [10–12] established a mathematical model for the flow rate of the quantitative axial piston pump, which considered the compressibility, the leakage of the fluid, and the damping groove of the port plate, and analyzed the flow and pressure characteristics of the piston chamber. Mandal et al. [13] analyzed the influence of the damping groove volume of manifold on pressure pulsation and flow pulsation. Bergada et al. [14] established a mathematical model for the axial piston pump which considered the swash plate angle, leakage gap, speed, and damping groove, and accurately modeled the pressure distribution characteristics in the port plate area during movement. The pressure distribution and flow leakage between the barrel block and the port plate and the force and torque of the barrel block were analyzed, and the double peaks of torque fluctuation were predicted. Tong et al. [15] used the Kane–Huston method to establish the multi-body dynamic model of the axial piston pump under mechanical–hydraulic coupling. According to the fluid characteristics and control principle of the axial piston pump, the hydraulic system model was established, and the joint virtual prototype was constructed. The motion characteristics, outlet flow and pressure pulsation characteristics, and flow control characteristics of the axial piston pump under mechanical–hydraulic coupling were analyzed. Bergada et al. [16] established the clearance leakage model of the axial

piston pump, and designed an experimental platform for the experimental study of the dynamic pressure of the piston chamber. The study showed that the main leakage sources of the axial piston pump were the port plate–barrel block pair and the slipper–swash plate pair. Fu et al. [17] established the simulation model of the electro-hydraulic pump and analyzed the flow characteristics of the electro-hydraulic pump. Xu et al. [18] established the simulation model of the axial piston pump based on cross-angle, and studied the influence of cross-angle on the inlet and outlet flow pulsation and piston chamber pressure.

In order to simulate the fluid characteristics of hydraulic volumetric machinery more accurately, Casoli et al. [19] analyzed the fluid modeling method in the numerical model of the swash plate axial piston pump. The research showed that the fluid model containing cavitation of gas and vapor is consistent with the experiment in a wider range of working conditions. Ye et al. [20] established a dynamic model of axial piston pump, which simulated the fluid characteristics in detail to reflect the air release and cavitation phenomenon, analyzed the causes and influencing factors of different noise sources, and studied the influence of port plate parameters on noise sources. Ouyang et al. [21] analyzed the difference in the pressure pulsation of the piston pump between the fully coupled model and the ordinary model, and discussed the causes of the swash plate vibration and its relationship with the pressure pulsation. Karpenko et al. [22] studied the hydrodynamic process characteristics in the hydraulic system “axial piston pump–pipeline–fittings”, and analyzed the fluid pulsation characteristics of the piston pump and the pressure loss at the fittings. Pan et al. [23] established the theoretical model of outlet flow and pressure pulsation of the constant power variable piston pump, analyzed the influence of swash plate vibration on outlet flow and pressure pulsation of the axial piston pump, and investigated the optimization of port plate based on the theoretical model of outlet flow pulsation. Wang et al. [24] established a dynamic model for the spring reset piston pump, and analyzed the leakage of plunger vice, motion state, pressure, and flow characteristics of the piston pump under different working conditions. Hong et al. [25,26] analyzed the influence of the depth angle and width angle of the triangular damping groove on the flow pulsation and the influence of the width radius, as well as the depth and length angle of the U-shaped damping groove on the flow pulsation. Furthermore, they proposed an evaluation criterion of the flow pulsation performance of the damping groove based on the time domain characteristics, and then optimized the structure of the damping groove of the port plate to reduce the flow pulsation at the outlet. Lyu et al. [27] proposed a method to reduce the harmonic amplitude of specific order flow pulsation by using piston non-uniform distribution. Deng et al. [28] established a kinematic model, a piston chamber pressure model, a dynamic model, and an external return spherical bearing pair lubrication model for the double-row axial piston pump, and studied the kinematic characteristics of the piston pump and the lubrication characteristics of external return mechanism under multiple working conditions. The research results of many scholars above show that the numerical simulation method has the characteristics of high efficiency and low cost in analyzing the dynamic characteristics of the axial piston pump compared with the experimental test, so the numerical simulation is a more efficient analysis method.

The double-compound axial piston pump adopts a power control mode, so the output flow can be adjusted according to the load pressure, and the flow variation is determined by the power control curve. Therefore, the dynamic characteristics of the double-compound axial piston pump are greatly affected by the working conditions. Most of the existing researches focus on the characteristics analysis of the quantitative piston pump or the variable piston pump with specific displacement. There are few studies on the control and dynamic characteristics of the power-controlled double-compound axial piston pump, and there is no analysis of the influence of working conditions on the dynamic characteristics, which greatly limits the analysis and optimization of flow pulsation, pressure shock, and vibration noise in the double-compound axial piston pump. In this study, by analyzing the working and control principle of the double-compound axial piston pump, the numerical model of the double-compound axial piston pump is established, and the numerical

simulation model is established and verified by experiments. The constant power control and variable power control characteristics of the double-compound axial piston pump are analyzed. By analyzing the dynamic characteristics of the double-compound axial piston pump, the influence law of different working conditions on the dynamic characteristics of the double-compound axial piston pump is clarified. It provides a theoretical basis and research basis for the analysis and optimization of power control and the analysis and control of flow pulsation and fluid vibration and noise of the double-compound axial piston pump.

2. Description of Physical System

The hydraulic system of the double-compound axial piston pump is shown in Figure 1. The pump is mainly composed of a front pump, a rear pump, a front pump controller, a rear pump controller, an intermediate, a pilot pump, and an electromagnetic proportional pressure-reducing valve. The control of the swash plate angle is a key objective of displacement control for the variable displacement pump. The control mode of the double-compound axial piston pump requires a combination of power control and negative flow control.

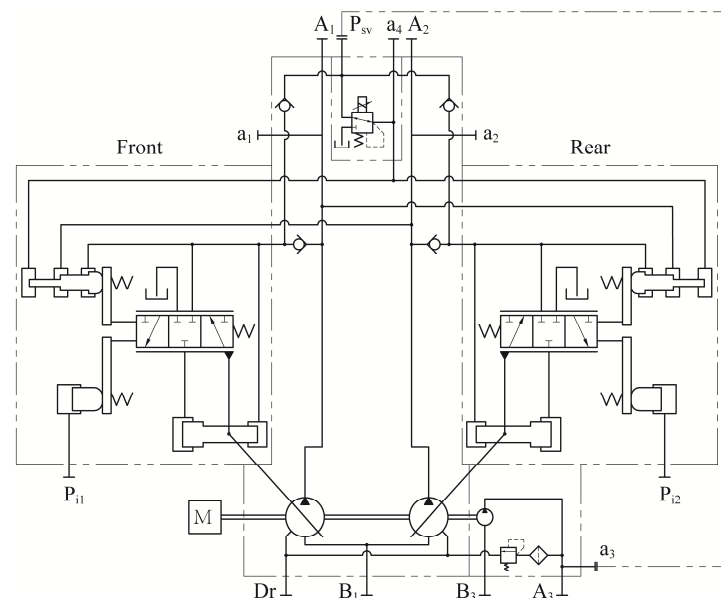


Figure 1. Principle diagram of the hydraulic system for the double-compound axial piston pump.

The structures of the front pump and the rear pump, the front pump controller, and the rear pump controller are the same, and are symmetrically installed relative to the intermediate. Figure 2 shows the internal structure of the front pump and the front pump controller. The pump has nine pistons, which are installed in the piston chamber of the barrel block. Each piston is hinged with the slipper through the ball head, and the slipper is pressed on the surface of the swash plate by the slipper retainer to maintain reasonable contact with the surface of the swash plate. The barrel block is connected to the spindle to make the piston and barrel block rotate relative to the port plate fixed on the intermediate.

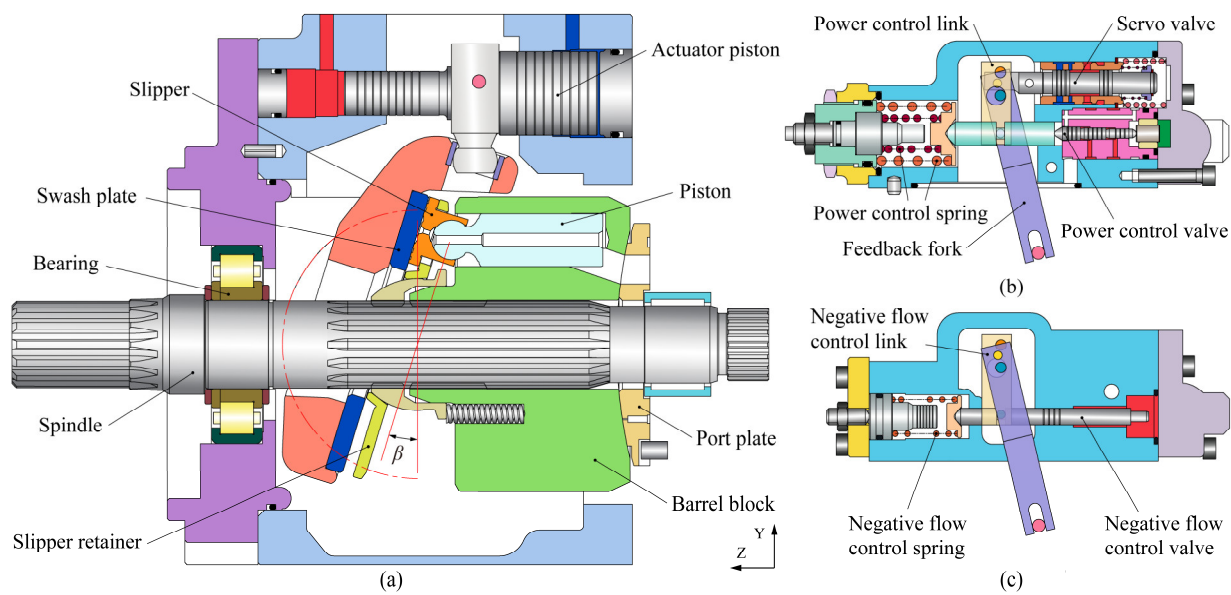


Figure 2. Structure diagram of the front pump and controller for the double-compound axial piston pump: (a) front pump; (b,c) front pump controller.

The port plate structure mainly includes inlet main groove, outlet main groove, and damping structure, as shown in Figure 3. Suppose the pump starts working when a piston is at zero baseline. When the volume of the piston chamber is the smallest, i.e., when the z -axis coordinate value of the piston is the smallest, this position of the piston is called the top dead center. When the volume of the piston chamber is the largest, i.e., when the z -axis coordinate value of the piston is the largest, this position of the piston is called the bottom dead center. The damping structure mainly includes the damping groove and the damping hole. In the process of connecting the opening groove of the piston chamber from the inlet main groove to the outlet main groove, the pre-compression operation of the low-pressure oil in the piston chamber is carried out using the two methods of closed mechanical compression and the introduction of high-pressure oil through the damping structure. In the process of connecting the opening groove of the piston chamber from the outlet main groove to the inlet main groove, part of the residual high-pressure oil in the piston chamber is extracted from the damping structure to the low-pressure area, and the other part is depressurized by the mechanical expansion of the piston chamber, so as to complete the pre-release pressure operation.

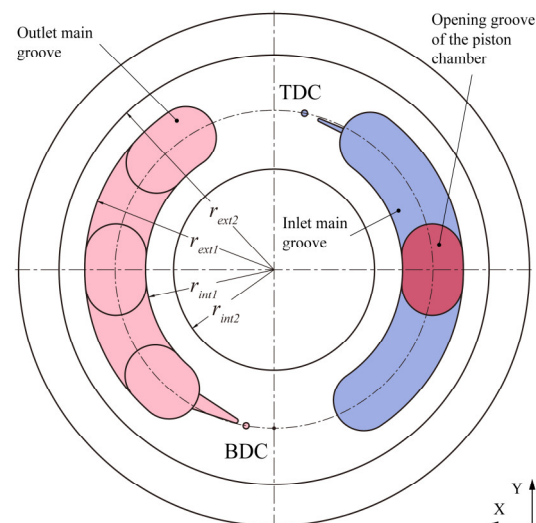


Figure 3. Port plate structure.

Power control means that when the working load of the double-compound axial piston pump is small, the output power of the piston pump (the sum of the power of the front pump and the rear pump) does not exceed the set power, and the piston pump works with the maximum displacement to ensure the rapid operation of small load. When the load increases and the output power of the piston pump exceeds the set power in advance, in order to avoid overload of the prime motor, it is necessary to reduce the displacement of the piston pump to realize heavy load and low speed operation and keep the power of the piston pump basically constant. Negative flow control means that the flow rate of the double-compound axial piston pump decreases with an increase in the pilot control pressure. When it is in the non-working state, reducing the output flow can effectively reduce the overflow loss and throttling loss.

The power control system is composed of a power control valve, a power control spring, a servo valve, a power control link, a feedback fork, and an actuator piston, as shown in Figure 2b. The power control valve core has two annular surfaces with equal action area, which are connected to the load oil circuit of the front pump and the rear pump, respectively. Therefore, the regulating force of the working load of the front pump and the rear pump on the power control system is equal. Then, the right end of the valve core is connected with the power control pilot pressure of the electromagnetic proportional pressure-reducing valve. When the piston pump starts to work, the swash plate reaches the maximum swash plate angle under the pilot pressure, so the pump starts with a large swash plate angle. The negative flow control system is composed of a negative flow control valve, a negative flow control spring, a negative flow control link, a feedback fork, and an actuator piston, as shown in Figure 2c. The right end of the negative flow control valve core is connected to the negative flow control pilot oil circuit.

Take the front pump as an example to illustrate the power control process of the double-compound axial piston pump, as shown in Figure 2. When the pressure on the right side of the power control valve core is small, the preload of the power control spring at the left end cannot be overcome. At this time, the power control valve core does not move, and the piston pump still outputs at the maximum displacement. When the load pressure gradually increases and reaches the power setting starting point, the power control valve core moves to the left, the outer spring of the power control spring is compressed, and the inner spring is still in a free state. Driven by the power control link and the feedback fork, the servo valve controls the working oil circuit to connect to the large cavity of the actuator piston. The actuator piston moves to the left, the inclination angle of the swash plate decreases, and the displacement of the piston pump decreases. While the displacement is reduced, the actuator piston drives the servo valve through the feedback fork to close the oil inlet channel of the large cavity in the actuator piston, and the adjustment is completed. As the power control valve core moves to the left, the output flow of the piston pump decreases rapidly with an increase in the load pressure. When the load pressure continues to increase, the core of the power control valve continues to move to the left, and the outer spring and inner spring of the power control spring act at the same time, changing the balance state of the force. At this time, the output flow of the piston pump decreases slowly with an increase in the load pressure. When the load pressure decreases, the core of the power control valve moves to the right, and the servo valve controls the execution of oil drainage in the large cavity of the actuator piston. When the actuator piston moves to the right, the inclination angle of the swash plate increases and the displacement of the piston pump increases. In order to achieve more precise operation requirements, the power of the piston pump can be reduced. At this time, the electromagnetic proportional reducing valve outputs a certain pilot pressure, and the force on the right end of the power control valve core increases. The power setting starting point of the piston pump decreases, the control curve moves to the left, and the output flow of the piston pump decreases under the same load pressure.

When the negative flow control pilot pressure on the right end of the negative flow control valve core is small, the preload of the negative flow control spring at the left end

cannot be overcome, and the negative flow control valve core does not move. When the pilot control pressure increases gradually and reaches the set starting point, the negative flow control valve core moves to the left. Driven by the negative flow control link and the feedback fork, the servo valve controls the working oil circuit to connect to the large cavity of the actuator piston. The actuator piston moves to the left, the inclination angle of the swash plate decreases, and the displacement of the piston pump decreases. When the pilot control pressure decreases, the negative flow control valve core moves to the right, and the servo valve controls the execution of oil drainage in the large cavity of the actuator piston. The actuator piston moves to the right, the inclination angle of the swash plate increases, and the displacement of the piston pump increases. The negative flow control pilot pressure is generally generated by the bypass pressure detection unit. Moreover, the bypass pressure detection unit is composed of a damping hole and its parallel overflow valve, and the damping hole is connected to the tank.

3. Numerical Model of the Double-Compound Axial Piston Pump

According to the physical system of the double-compound axial piston pump, the dynamic model and control model of the double-compound axial piston pump are established.

3.1. Dynamic Model of Axial Piston Pump Body

Each piston chamber is modeled as a capacitive volume model, as shown in Figure 4, and its pressure is obtained by integrating the expression of time derivative [9,29]. Different from the models established in previous studies, the model established in this study regards the leakage of the slipper–swash plate pair and the piston–barrel block pair as coming from the piston chamber, and the leakage of the port plate–barrel block pair as coming from the oil suction chamber and the oil discharge chamber. Therefore, only the slipper–swash plate pair and the piston–barrel block pair are considered in the oil leakage in the capacitive volume model of the piston chamber, and the transient pressure in the piston chamber is expressed as:

$$\frac{dp_{p,i}}{dt} = \frac{E}{V_{p,i}} \left(-Q_{pin,i} - Q_{pout,i} - Q_{lpbb,i} - Q_{lssp,i} - \frac{dV_{p,i}}{dt} \right) \quad (1)$$

where $p_{p,i}$ is the pressure of piston chamber, $V_{p,i}$ is the volume of piston chamber, E is the bulk modulus of hydraulic oil, $Q_{pout,i}$ is the outlet flow of piston chamber, $Q_{pin,i}$ is the inlet flow of piston chamber, $Q_{lpbb,i}$ is the leakage flow of the piston–barrel block pair, and $Q_{lssp,i}$ is the leakage flow of the slipper–swash plate pair.

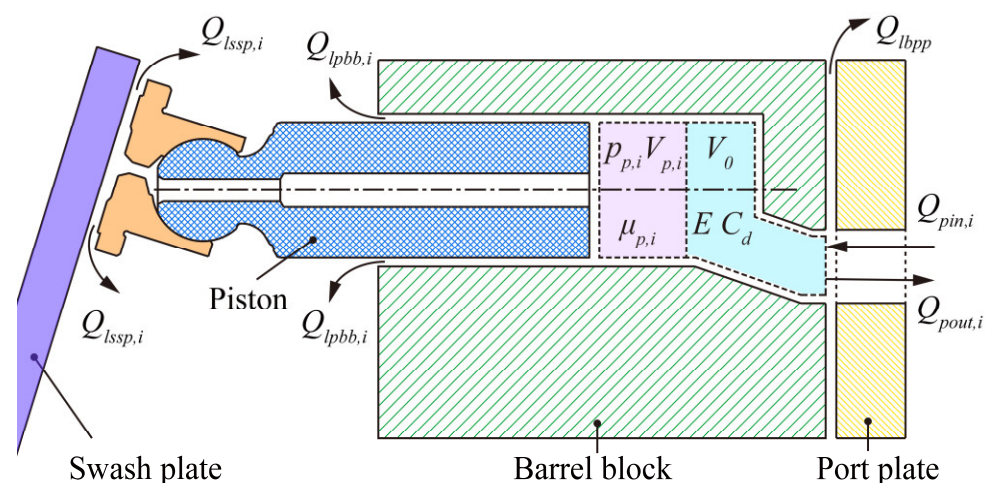


Figure 4. Model of the piston chamber.

Between the piston chamber and the port plate is regarded as a thin-walled hole. Therefore, the flow between the piston chamber and the inlet and outlet of the port plate is turbulent. The flow $Q_{pout,i}$ and $Q_{pin,i}$ through the orifice are expressed as [9]:

$$\begin{cases} Q_{pin,i} = C_d A_{pin,i} \sqrt{\frac{2|p_{p,i} - p_s|}{\rho}} \text{sign}(p_{p,i} - p_s) \\ Q_{pout,i} = C_d A_{pout,i} \sqrt{\frac{2|p_{p,i} - p_d|}{\rho}} \text{sign}(p_{p,i} - p_d) \end{cases} \quad (2)$$

where p_d is the pump outlet pressure, p_s is the pump inlet pressure, C_d is the flow coefficient, $A_{pin,i}$ is the flow area between the inlet main groove and the i th piston chamber, and $A_{pout,i}$ is the flow area between the outlet main groove and the i th piston chamber.

The piston makes compound movement with the main shaft, and the volume of the piston chamber is expressed as:

$$V_{p,i} = V_0 + V_1 + \frac{\pi}{4} d_p^2 R \tan \beta \sin(\omega t) \quad (3)$$

$$V_1 = \frac{\pi d_p^2}{4} R \tan \beta_{\max} \quad (4)$$

where d_p is the piston diameter, R is the piston distribution radius, β is the inclination angle of the port plate, ω is the rotational speed of the spindle, V_0 is the structure dead volume of the piston chamber, and V_1 is the volume of the piston cavity at zero position.

The flow rate of piston chamber generated by piston movement is expressed as:

$$Q_{p,i} = \frac{dV_{p,i}}{dt} = \frac{\pi d_p^2}{4} [\omega R \tan \beta \cos(\omega t) + \beta' R \sec^2 \beta \sin(\omega t)] \quad (5)$$

The internal kinematic pair leakage of axial piston pump is mainly composed of three parts: piston–barrel block pair leakage, slipper–swash plate pair leakage, and port plate–barrel block pair leakage [16]. In order to accurately calculate the outlet flow rate, it is necessary to numerically calculate the leakage of the piston–barrel block pair, the slipper–swash plate pair, and the port plate–barrel block pair. The total leakage flow is expressed as:

$$Q_l = \sum_{i=1}^N Q_{lpbb,i} - \sum_{i=1}^N Q_{lssp,i} - Q_{lppb} \quad (6)$$

where Q_{lppb} is the leakage flow of the port plate–barrel block pair.

The leakage flow of the piston–barrel block pair is obtained as:

$$Q_{lpbb,i} = \frac{\pi d_p h_p}{4 \mu_{p,i} l_{pc,i}} (p_{p,i} - p_c) \left(\frac{h_p^2}{24} + \frac{e_p^2}{4} \right) + \frac{\pi d_p h_p}{2} u_{p,i} \quad (7)$$

where h_p is the diameter gap between the piston and the piston chamber, e_p is the eccentricity distance between the piston and the piston chamber, $l_{pc,i}$ is the contact length between the piston and the piston chamber, $\mu_{p,i}$ is the dynamic viscosity of the piston–barrel block pair gap, and $u_{p,i}$ is the Couette effect of the piston speed on the leakage flow.

The leakage flow of the slipper–swash plate pair is obtained as [13]:

$$Q_{lssp,i} = \frac{\pi (p_{p,i} - p_c) h_{ssp}^3 d_{tp}^4}{\mu_{p,i} [6 d_{tp}^4 \ln(r_{spo}/r_{spi}) + 128 h_{ssp}^3 l_{tp}]} \quad (8)$$

where h_{ssp} is the gap between slipper and swash plate, d_{tp} is the diameter of piston damping orifice, l_{tp} is the length of the piston damping orifice, r_{spo} is the outer radius of the slipper, and r_{spi} is the inner radius of the slipper.

The leakage of the port plate–barrel block pair is divided into two parts: the leakage $Q_{l_{pbi}}$ between the port plate inlet and the barrel block and the leakage $Q_{l_{pbo}}$ between the port plate outlet and the barrel block. The leakage caused by triangular damping grooves should also be included, but the studies of Bergada et al. [14,16] show that such leakage can be negligible compared with the port plate main groove. The leakage flow of port plate–barrel block pair is obtained as [14]:

$$Q_{l_{ppb}} = Q_{l_{pbi}} + Q_{l_{pbo}} = -\frac{\theta_{in}h_{ppb}^3(p_s - p_c)}{12\mu} \left(\frac{1}{\ln(r_{ext1}/r_{ext2})} - \frac{1}{\ln(r_{int1}/r_{int2})} \right) - \frac{\theta_{out}h_{ppb}^3(p_d - p_c)}{12\mu} \left(\frac{1}{\ln(r_{ext1}/r_{ext2})} - \frac{1}{\ln(r_{int1}/r_{int2})} \right) \tag{9}$$

where p_c is the pressure of leakage cavity, h_{ppb} is the gap between the barrel block and the port plate, θ_{in} is the angle range of the inlet main groove of the port plate, θ_{out} is the angle range of the outlet main groove of the port plate, r_{int1} is the outer radius of the internal port plate, r_{int2} is the inner radius of the internal port plate, r_{ext1} is the inner radius of the external port plate, r_{ext2} is the outer radius of the external port plate, and μ is the dynamic viscosity.

The inlet and outlet flow of the pump is the sum of the inlet and outlet flow of all the piston chamber through the port plate. The phase angle of each piston is considered:

$$Q_{in} = \sum_{i=1}^N Q_{pin,i(\phi_i)} - Q_{l_{pbi}} \tag{10}$$

$$Q_{out} = \sum_{i=1}^N Q_{pout,i(\phi_i)} - Q_{l_{pbo}} \tag{11}$$

Given the working conditions of the inlet and outlet of the pump, the power input of the spindle and the working state of the swash plate, the model can calculate the pressure of the piston chamber according to Equation (1), and then calculate the inlet and outlet flow of each piston chamber by using the equation. Finally, Equations (6), (10) and (11) are used to calculate the leakage flow and the inlet and outlet flow of the piston pump.

The oil pressure in each piston chamber acts on the bottom surface of the piston, and the equivalent force $F_{p,i}$ is applied to the middle of the bottom surface of the piston and is perpendicular to it (i.e., along the z axis). The viscous friction $F_{vl_{pc,i}}$ caused by the leakage of the piston–barrel block pair is also applied to the piston along the z axis.

$$\begin{cases} F_{p,i} = p_{p,i} \frac{d_p^2}{4} \\ F_{vl_{pc,i}} = 2\pi(d_p - h_p) \left(\frac{p_{p,i} - p_c}{8} h_p - \frac{1}{h_p} \mu_{p,i} l_{pc,i} u_{p,i} \right) \end{cases} \tag{12}$$

Therefore, the resultant force acting on each piston is obtained as:

$$F_{pt,i} = F_{p,i} + F_{vl_{pc,i}} \tag{13}$$

The viscous friction generated by the rotation of each slipper on the swash plate is obtained as:

$$F_{vls,i} = \frac{\pi \mu_{p,i} \omega R}{h_{ssp}} (r_{spo}^2 - r_{spi}^2) \tag{14}$$

The torque applied by the piston to the swash plate is obtained as:

$$T_{sp} = \sum_{i=1}^N y_{p,i} (F_{ptz,i} + F_{vlsz,i}) - \sum_{i=1}^N z_{p,i} (F_{pty,i} + F_{vlsy,i}) \tag{15}$$

where $y_{p,i}$ is the force arm of the resultant force along the z axis in the y direction, $z_{p,i}$ is the force arm of the resultant force along the y axis in the z direction, $F_{ptz,i}$ and $F_{pty,i}$ are

the projections of the resultant force $F_{pt,i}$ on the z and y axis, and $F_{vlsz,i}$ and $F_{vlsy,i}$ are the projections of the resultant force $F_{vls,i}$ on the z and y axis.

The viscous friction torque between the port plate and the barrel block is obtained as:

$$T_{vlpp} = \frac{\theta_{in}\mu\omega}{4h_{ssp}} \left[(r_{int1}^4 - r_{int2}^4) + (r_{ext1}^4 - r_{ext2}^4) \right] + \frac{\theta_{out}\mu\omega}{4h_{ssp}} \left[(r_{int1}^4 - r_{int2}^4) + (r_{ext1}^4 - r_{ext2}^4) \right] \quad (16)$$

Therefore, the spindle torque of piston pump is obtained as:

$$T_{sf} = \sum_{i=1}^N x_{p,i} (F_{pty,i} + F_{vlsz,i}) - \sum_{i=1}^N y_{p,i} F_{vlsx,i} + T_{vlpp} \quad (17)$$

In the actual hydraulic system, hydraulic oil always contains some gas, which is air in most cases. In a hydraulic system, when the pressure somewhere of the liquid is lower than saturation pressure (or air separation pressure) P_{sat} , the air dissolved in the liquid is released, and a large number of bubbles are produced in the liquid, which is called aeration (or air separation). Aeration is very important in hydraulic system simulation. In addition, there is a separate phenomenon called cavitation. When the fluid pressure decreases to a certain value, the fluid evaporates and produces a large amount of vapor, which is called cavitation. This happens when the pressure reaches saturated vapor pressure. Generally, the chemical properties of the fluid are not pure, so cavitation does not occur under a single pressure, but within a certain pressure range [19,30]. Therefore, the pressure at the beginning of cavitation is called high-saturation vapor pressure P_{vap}^H , and the pressure at the completion of cavitation is called low-saturation vapor pressure P_{vap}^L .

When the pressure of hydraulic oil is higher than the saturation pressure, the air is completely dissolved in the hydraulic oil, as shown in Figure 5. When the pressure of hydraulic oil is lower than the saturation pressure, the air begins to separate out, and part of the air in the hydraulic oil is dissolved and partially free. When the pressure of hydraulic oil is lower than the high-saturation vapor pressure, the hydraulic oil begins to evaporate to produce vapor. When the pressure continues to decrease to low-saturation vapor pressure, the hydraulic oil is completely vaporized, and only air and vapor exist. Aeration and cavitation can not be ignored for axial piston pump, so these phenomena are considered in the double-compound axial piston pump model. The modeling of fluid properties, as described in IMAGING [30], takes these phenomena into account.

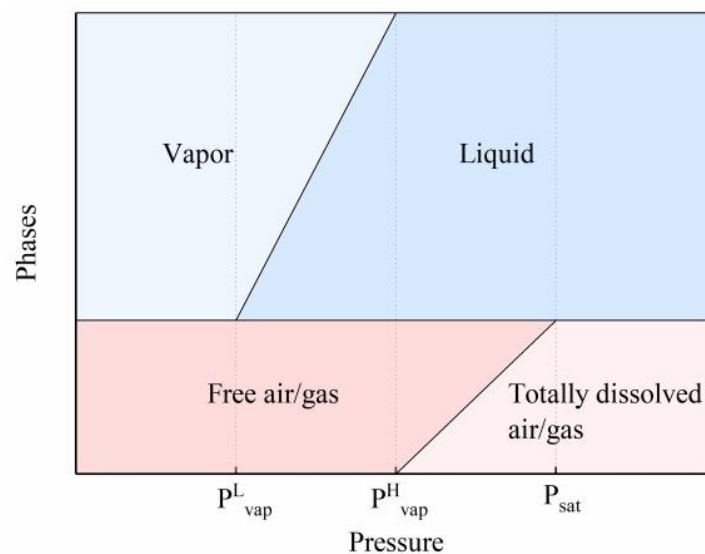


Figure 5. Model of fluid characteristic.

3.2. Model of Swash Plate Variable Displacement Control

The diagram of the linkage mechanism is obtained by simplifying the structure of the double-compound axial piston pump controller, showing the pin position points on the linkage mechanism, as shown in Figure 6. The power control process and negative flow control process are obtained by analyzing the principle of the power control and negative flow control of the double-compound axial piston pump, as shown in Figures 7 and 8.

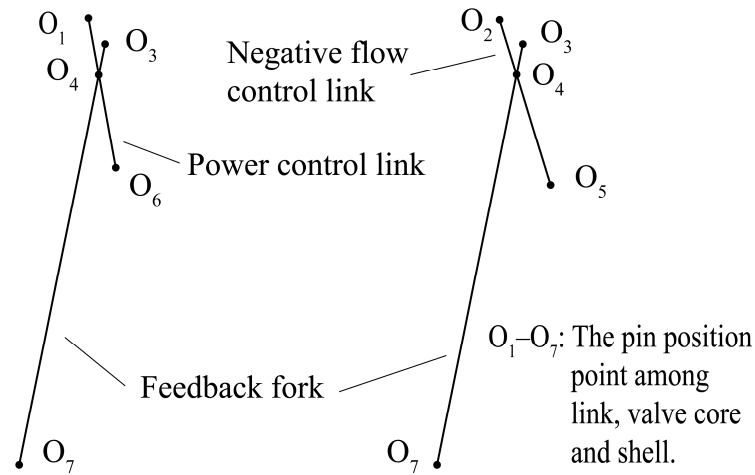


Figure 6. Diagram of the linkage mechanism.

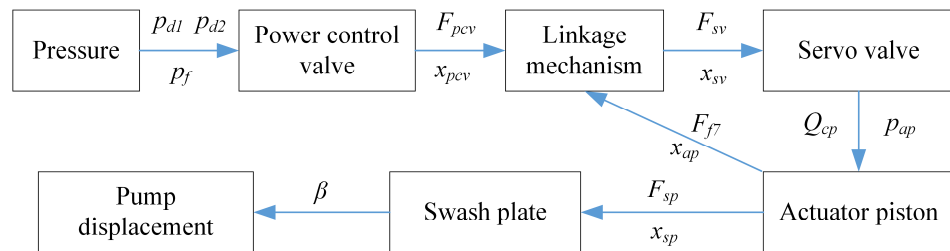


Figure 7. Flow chart of the power control.

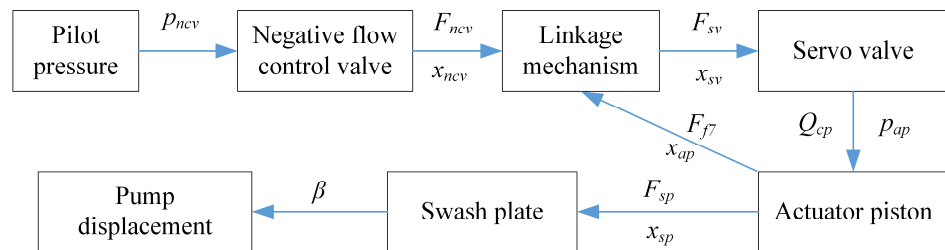


Figure 8. Flow chart of the negative flow control.

In the process of power control, according to the motion relationship between the power control valve, the servo valve, and linkage mechanism, the motion equation of servo valve is expressed as:

$$p_f A_f + p_{d1} A_{pcv1} + p_{d2} A_{pcv2} - F_{pcv0} - F_{sv0} / k_3 k_4 = a_1 \ddot{x}_{sv} + a_2 \dot{x}_{sv} + a_3 x_{sv} \quad (18)$$

$$a_1 = m_{pcv} k_3 k_4 + J_1 k_3 k_4 / l_1^2 + J_{f7} / k_3 k_4 l_4^2 + m_{sv} / k_3 k_4 \quad (19)$$

$$a_2 = c_{pcv} k_3 k_4 + c_{sv} / k_3 k_4 \quad (20)$$

$$a_3 = k_{pcv} k_3 k_4 + k_{sv} / k_3 k_4 \quad (21)$$

where p_{d1} is the load pressure of the front pump, p_{d2} is the load pressure of the rear pump, p_f is the power control pilot pressure, A_{pcv1} is the effective area of the load pressure of the front pump acting on the power control valve, A_{pcv2} is the effective area of the load pressure of the rear pump acting on the power control valve, A_f is the effective area of the power control pilot pressure acting on the power control valve, F_{pcv0} is the spring preload of the power control valve, F_{sv0} is the spring preload of the servo valve, x_{sv} is the displacement of the servo valve, m_{pcv} is the mass of power control valve core, and m_{sv} is the mass of servo valve core. J_1 is the moment of inertia of the power control link around O_1 ; J_7 is the moment of inertia of feedback fork around O_7 ; $k_3 = l_1/l_2$, $k_4 = l_3/l_4$, l_1 is the distance between O_1 and O_6 ; l_2 is the distance between O_1 and O_4 ; l_3 is the distance between O_4 and O_7 ; l_4 is the distance between O_3 and O_7 ; c_{pcv} is the damping coefficient of the power control valve; c_{sv} is the damping coefficient of the servo valve; k_{sv} is the spring stiffness of the servo valve; and k_{pcv} is the spring stiffness of the power control valve.

$$k_{pcv} = \begin{cases} k_1, & 0 \leq x_{pcv} \leq x_0, \\ k_1 + k_2, & x_0 \leq x_{pcv} \leq x_{lim}. \end{cases} \quad (22)$$

where x_{pcv} is the displacement of the power control valve core, x_0 is the distance difference between the zero position of the double springs of the power control valve, k_1 is the spring stiffness of the outer spring of the power control valve, k_2 is the spring stiffness of the inner spring of the power control valve, and x_{lim} is the maximum displacement of the power control valve core.

According to the motion relationship between the actuator piston, linkage mechanism, and servo valve, the feedback motion equation of servo valve is expressed as:

$$p_{ap}A_d - p_dA_x - (1/k_4 - 1)F_{sv0} - F_{sp} = a_4\ddot{x}_{svf} + a_5\dot{x}_{svf} + a_6(x_{sv} - x_{svf}) \quad (23)$$

$$a_4 = m_{ap}k_4/(1 - k_4) + J_{f4}k_4/l_3^2(1 - k_4) + m_{sv}(1/k_4 - 1) \quad (24)$$

$$a_5 = c_{ap}k_4/(1 - k_4) + c_{sv}(1/k_4 - 1) \quad (25)$$

$$a_6 = k_{sv}(1/k_4 - 1) \quad (26)$$

where p_{ap} is the pressure of the large cavity of the actuator piston, A_d is the action area of the large cavity of the actuator piston, A_x is the action area of the small cavity of the actuator piston, F_{sp} is the force of the swash plate on the actuator piston, x_{svf} is the feedback displacement of the servo valve, m_{ap} is the mass of the actuator piston, J_{f4} is the moment of inertia of feedback fork around O_4 , and c_{ap} is the damping coefficient of the actuator piston.

The flow continuity equation between the servo valve and actuator piston is expressed as:

$$k_q(x_{sv} - x_{svf}) - k_c p_{ap} = A_d \dot{x}_{ap} + c_{ap} p_{ap} + \frac{V_{ap}}{\beta} \frac{dp_{ap}}{dt} \quad (27)$$

$$k_q = C_d w_{sv} \sqrt{(p_{ap} - p_s)/\rho} \quad (28)$$

$$k_c = C_d w_{sv} (x_{sv} - x_{svf}) / 2 \sqrt{(p_{ap} - p_s)/\rho} \quad (29)$$

where x_{ap} is the displacement of the actuator piston, k_q is the flow gain of the servo valve, k_c is the flow–pressure coefficient of the servo valve, V_{ap} is the volume of the large cavity of the actuator piston, and w_{sv} is the flow area of the servo valve.

The motion equation of the swash plate is expressed as:

$$F_{sp}L_{sp} - T_{sp} = J_{sp} \frac{d^2\beta}{dt^2} + c_{sp} \frac{d\beta}{dt} \quad (30)$$

where L_{sp} is the acting force arm of the actuator piston to the swash plate, J_{sp} is the moment of inertia of the swash plate, and c_{sp} is the damping coefficient of the swash plate.

In the process of negative flow control, according to the motion relationship between the negative flow control valve, the servo valve, and linkage mechanism, the motion equation of servo valve is expressed as:

$$p_{ncv}A_{ncv} - F_{ncv0} - F_{sv0}/k_3k_4 = a_7\ddot{x}_{sv} + a_8\dot{x}_{sv} + a_9x_{sv} \quad (31)$$

$$a_7 = m_{ncv}k_4k_5 + J_2k_4k_5/l_5^2 + J_{f7}/(k_4k_5l_4^2) + m_{sv}/k_4k_5 \quad (32)$$

$$a_8 = c_{ncv}k_4k_5 + c_{sv}/k_4k_5 \quad (33)$$

$$a_9 = k_{ncv}k_4k_5 + k_{sv}/k_4k_5 \quad (34)$$

where p_{ncv} is the negative flow control pilot pressure; A_{ncv} is the effective area of the negative flow control pilot pressure acting on the negative flow control valve; F_{ncv0} is the spring preload of the negative flow control valve; m_{ncv} is the mass of the negative flow control valve core; J_2 is the moment of inertia of the negative flow control link around O_2 ; $k_5 = l_5/l_6$, l_5 is the distance between O_2 and O_5 ; l_6 is the distance between O_2 and O_4 ; c_{ncv} is the damping coefficient of the negative flow control valve; and k_{ncv} is the spring stiffness of the negative flow control valve.

The feedback equation of the servo valve, the flow continuity equation between the servo valve and the actuator piston, and the motion equation of the swash plate in the negative flow control process are the same as those in the power control process.

4. Numerical Simulation Model and Experimental Verification

According to the dynamic model of the axial piston pump body in the previous section, the equations are compiled based on AMESet as the sub-model of the axial piston pump. According to the model of swash plate variable displacement control, the variable control sub-models of front pump and rear pump are established based on AMESim. Furthermore, the numerical simulation model of the 115×2 double-compound axial piston pump is established. The specifications of this type of double-compound axial piston pump and the properties of hydraulic oil are shown in Tables 1 and 2. The model consists of an axial piston pump sub-model, a variable control sub-model, a simulated loading sub-model, and a simulated data collection sub-model, as shown in Figure 9. The simulation loading sub-model is mainly composed of a safety valve, a reversing valve, a load cylinder, and a bypass pressure detection unit.

Table 1. Specifications of the 115×2 double-compound axial piston pump.

Displacement (mL/r)	Speed (rpm)		Pressure (bar)		Flow (L/min)	
	Rated	Max.	Rated	Peak	Max.	Min.
$2 \times 115 \pm 2$	1800	2700	343	400	$2 \times 207 \pm 3$	$2 \times 30 \pm 3$

Table 2. Properties of hydraulic oil.

Parameter	Value
Density (kg/m ³)	876
Dynamic viscosity(Pa·s)	5.1×10^{-2}
Bulk modulus (MPa)	1700
Temperature (°C)	40~60
Gas content	0.1%
Saturation pressure (MPa)	7.1×10^{-2}
High-saturation vapor pressure (MPa)	3.3×10^{-3}
Low-saturation vapor pressure (MPa)	1.8×10^{-3}

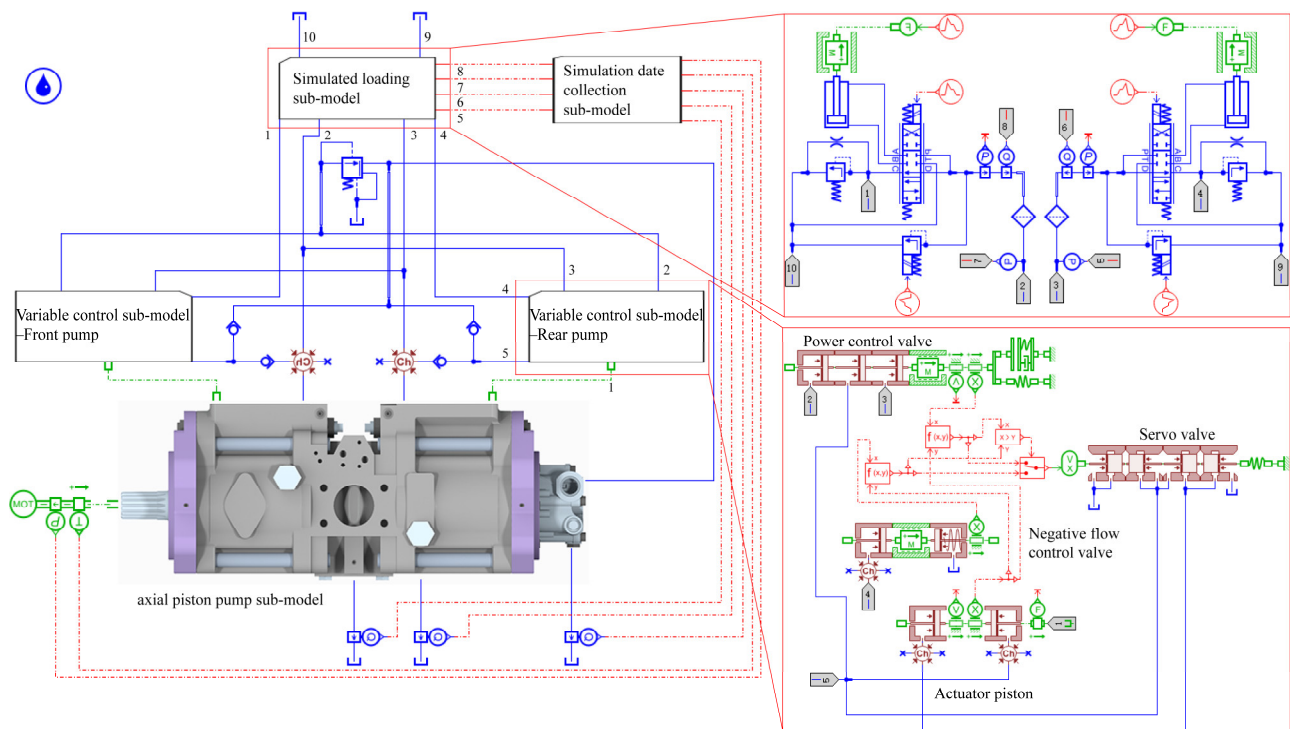


Figure 9. Numerical simulation model of the double-compound axial piston pump.

The double-compound axial piston pump is taken as the experimental object, verifying the accuracy and reliability of the numerical simulation model of double-compound axial piston pump. Figures 10 and 11 show the schematic diagram and test rig of the double-compound axial piston pump performance test system. The front pump, rear pump, and pilot pump of the tested pump are jointly driven by the prime mover and loaded by the electromagnetic proportional relief valve. Pilot pressure is generated by the pilot pump and the pilot pressure unit. The oil recovery unit is used to filter and recover the external leaked oil. In order to protect staff safety and reduce the impact of the test system on the surrounding environment, the whole hydraulic system hardware is enclosed in the isolation box, as shown in Figure 11a. The sensors, listed in Table 3, are installed on the test rig to measure the spindle speed and torque, outlet flow, pressure, leakage flow, and so on. The test rig allows the tested pump to adjust its rotational speed, load pressure, pilot control pressure, etc.

Table 3. Technical characteristics of measuring sensors.

Tag	Sensor	Range	Accuracy
n, T	Torque speed sensor	0~4000 r/min, 0~2000 N·m	0.2% F·S
P1, P2	Pressure transmitter	0~450 bar	0.125% F·S
P3, P6, P7, P8, P9	Pressure transmitter	0~60 bar	0.125% F·S
P4	Pressure transmitter	0~10 bar	0.125% F·S
P5	Pressure transmitter	-1~+5 bar	0.125% F·S
Q1, Q2	Flow meter	1.5~525 L/min	0.3% F·S
Q3, Q4	Flow meter	0.03~40 L/min	0.3% F·S
θ1	Temperature sensor	-40~350 °C	±1.0 °C

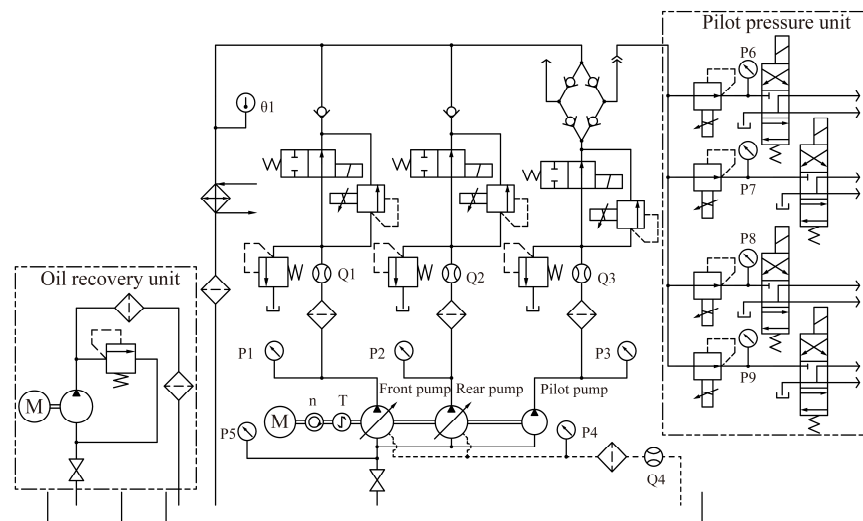


Figure 10. Schematic diagram of performance test system for the double-compound axial piston pump.

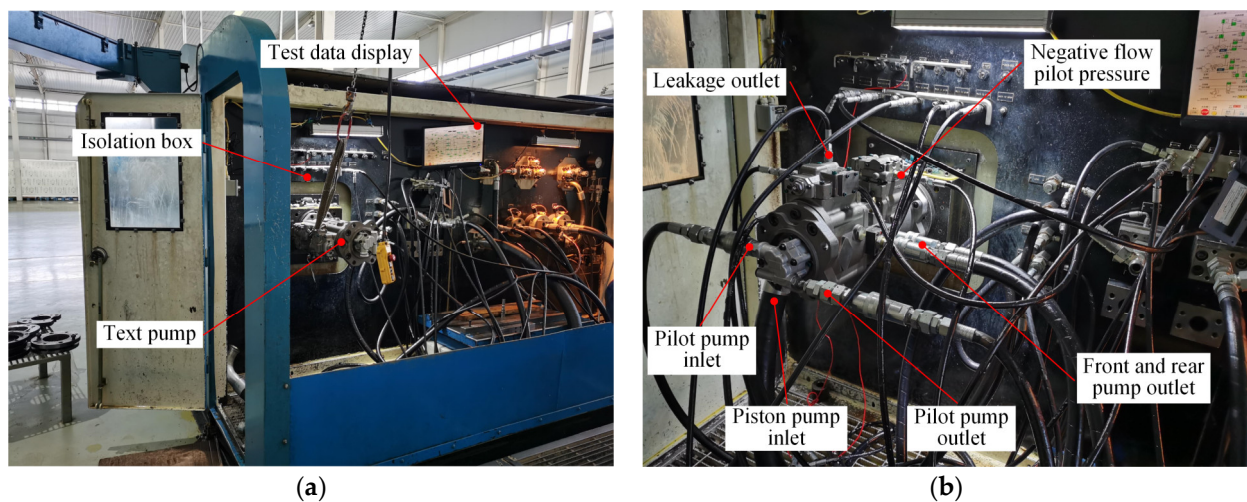


Figure 11. Performance test system for the double-compound axial piston pump: (a) test rig; (b) tested pump.

In order to verify the numerical simulation model, numerical simulation and experimental test are carried out under the same working conditions. For this purpose, three working conditions are set: condition 1 (power control, spindle speed is 1800 rpm, power control pilot pressure is 0.0 bar), condition 2 (power control, spindle speed is 1750 rpm, power control pilot pressure is 4.3 bar), and condition 3 (negative flow control, spindle speed is 1800 rpm, load pressure is 78 bar).

Figures 12–14 show the results of numerical simulation and experimental test of the double-compound axial piston pump under conditions 1, 2, and 3. Under the same working conditions, there is a certain deviation between the output flow of the front pump and the rear pump before the power setting starting point, as shown in Figure 12a. This deviation is mainly caused by the error of the actuator piston limit. The deviation of the second inflection point in the control curve between the experimental results and the simulation results is mainly caused by the setting error of the distance difference between the zero position of the double springs of the power control valve. Under the negative flow control mode, there is a significant difference between the upstream flow and the downstream flow, as shown in Figure 14a. This phenomenon is called hysteresis, and the flow hysteresis is mainly caused by the positive cover of the servo valve. Figure 15 shows the relative error

between the experimental results and simulation results under various working conditions. Under working condition 1, the relative error of flow calculation is less than 4.66%, and the relative error of torque calculation in a large working range is less than 3.10%. Under condition 2, the flow calculation error is less than 9.35%, and the torque calculation error is less than 11.28%. Under condition 3, the relative error of flow calculation is less than 5.20%. The design results, experimental results, and simulation results of characteristic flow points under three working conditions are shown in Table 4. The experimental results and simulation results of the flow value of characteristic points are basically within the design range, and there is a small deviation in the flow value of individual points, but this deviation is acceptable.

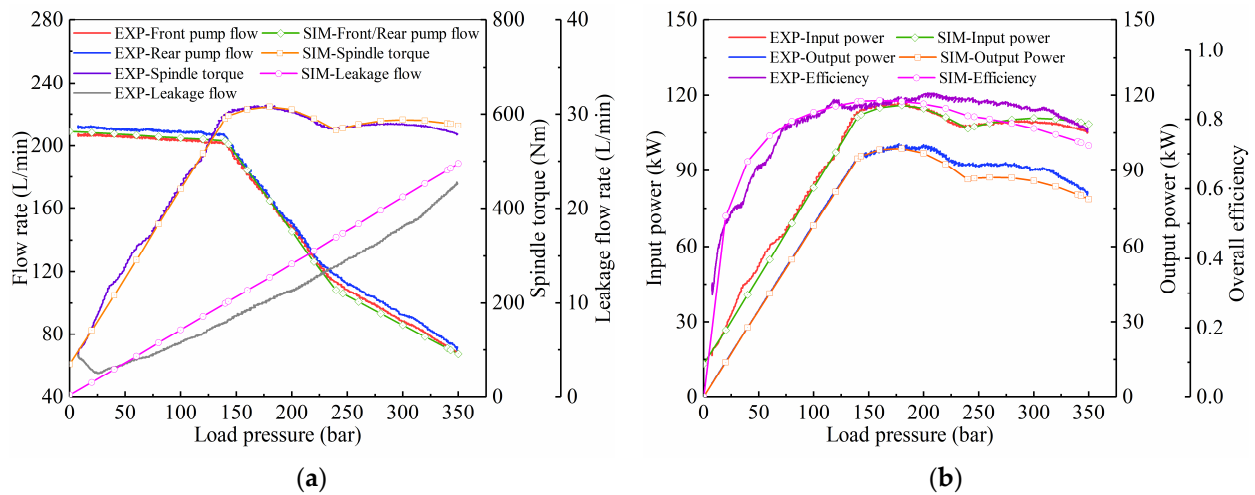


Figure 12. Characteristics curves of the double-compound axial piston pump under working condition 1: (a) outlet flow, spindle torque, and leakage flow; (b) input power, output power, and overall efficiency.

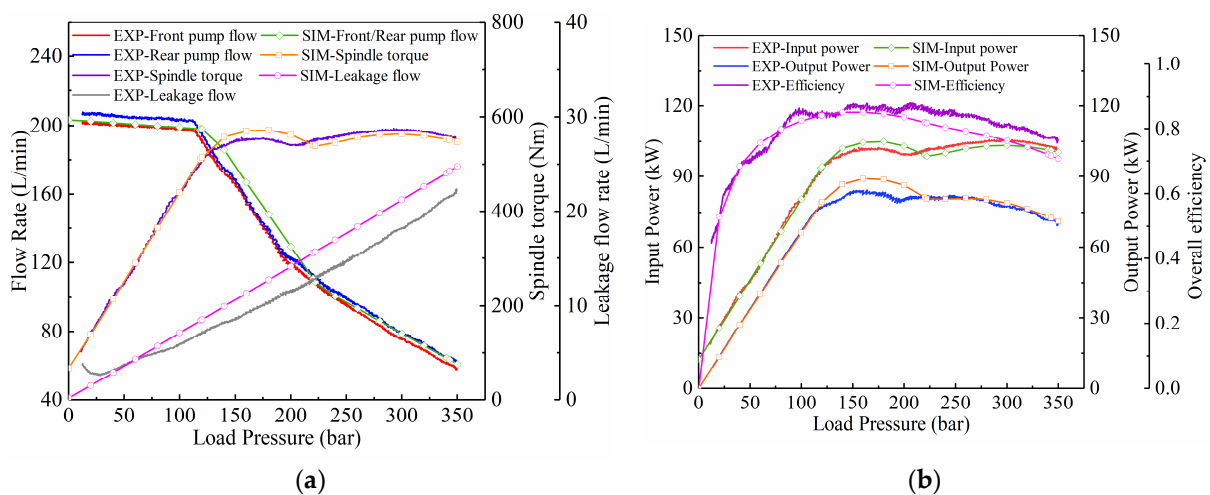


Figure 13. Characteristics curves of the double-compound axial piston pump under working condition 2: (a) outlet flow, spindle torque, and leakage flow; (b) input power, output power, and overall efficiency.

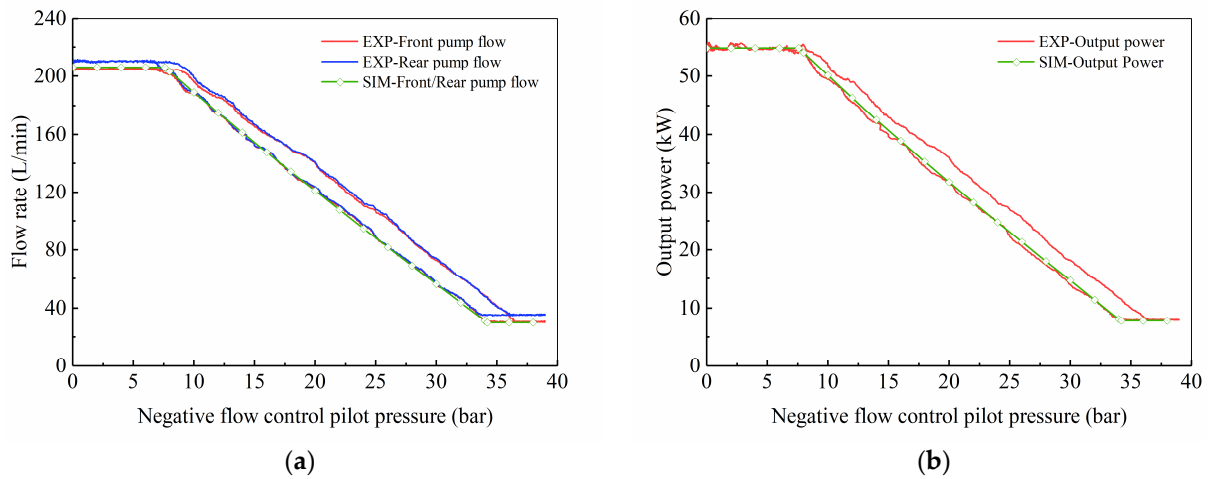


Figure 14. Characteristics curves of the double-compound axial piston pump under working condition 3: (a) outlet flow; (b) output power.

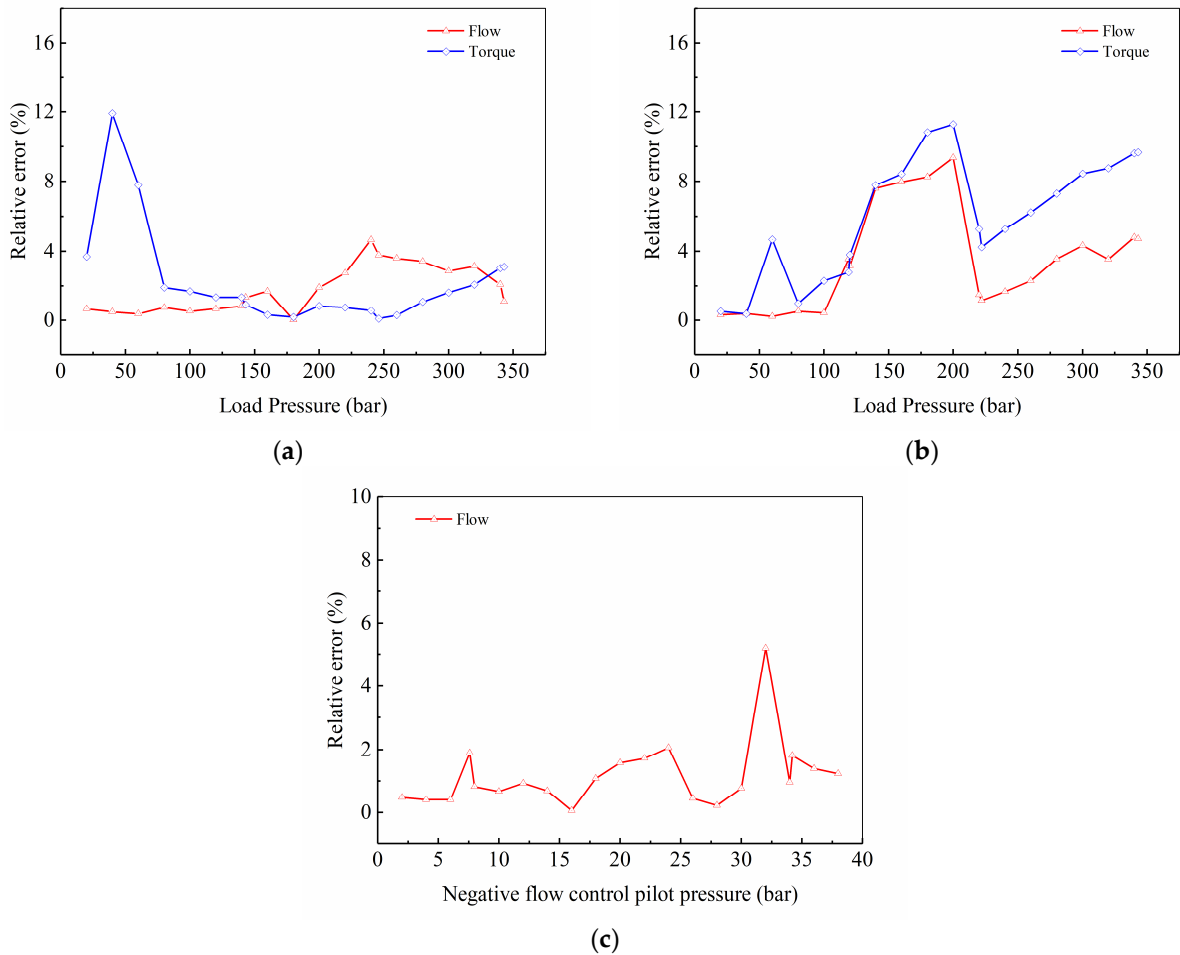


Figure 15. Error between experimental results and simulation results: (a) condition 1; (b) condition 2; (c) condition 3.

Table 4. Design value, test value, and simulation value of characteristic flow points.

Condition No.	Load Pressure/Pilot Pressure (bar)	Flow (L/min)		
		Design	Experiment	Simulation
1	143	202 ± 5	198.39	201.03
	246	111 ± 5	110.11	105.94
	343	75 ± 5	70.75	69.97
2	119	198 ± 5	195.81	198.21
	222	108 ± 5	113.08	110.80
	343	66 ± 5	64.93	63.43
3	7.6	205 ± 3	202.15	205.98
	34.2	30 ± 3	30.62	30.06

The curves of outlet flow, spindle torque, leakage flow, power, and overall efficiency obtained by the numerical simulation and experimental test are compared. The numerical simulation and experimental test results show the same trend, and the numerical simulation results are in good agreement with the experimental results, and the error is within the allowable range. Therefore, the numerical simulation method is accurate and reliable for the characteristics analysis of the double-compound axial piston pump. The numerical simulation model of the double-compound axial piston pump established in this paper is accurate and effective for the analysis of the static, dynamic, and control characteristics of the double-compound axial piston pump.

5. Analysis of Control Characteristics of the Double-Compound Axial Piston Pump

5.1. Analysis of Constant Power Control Characteristics

When the spindle speed and power control pilot pressure are determined, the upper power limit of the double-compound axial piston pump is determined. The numerical simulation of the double-compound axial piston pump is carried out under different setting power. The working conditions are shown in Table 5.

Table 5. Parameters of working conditions.

Condition No.	1	2	3	4	5	6
Pilot pressure p_f (bar)	0.0	2.8	4.3	5.9	9.0	9.0
Spindle speed n (rpm)	1800	1800	1750	1700	1600	1500

Figure 16 shows the constant power control curves of the double-compound axial piston pump under different working conditions. The outlet flow curve is in a three-section linear shape, and there are two inflection points on the curve. The first inflection point is the power setting starting point. The curve of spindle torque and input power after the power setting starting point is bimodal. The valley of the bimodal is the second inflection point of the flow curve, and the difference between the peak and valley is small. It can be considered that the power after the power setting starting point is basically constant. At the same spindle speed, with an increase in the power control pilot pressure, the power setting starting point decreases. Before the power setting starting point, the power control pilot pressure has no effect on the spindle torque. However, after the power setting starting point, the spindle torque decreases with an increase in the power control pilot pressure. The input power of the pump shows the same trend as the spindle torque. Under the same power control pilot pressure, a decrease in the spindle speed has no effect on power setting starting point, but the output flow decreases with a decrease in the spindle speed. The spindle torque is basically not affected by the spindle speed, but the input power decreases with a decrease in the spindle speed. The power control pilot pressure controls the left and right movement of the flow curve, while the spindle speed controls the up-and-down movement of the flow curve. Both the power control pilot pressure and the spindle speed

affect the input power, but the spindle speed has no effect on the spindle torque, and the spindle torque is only affected by the power control pilot pressure.

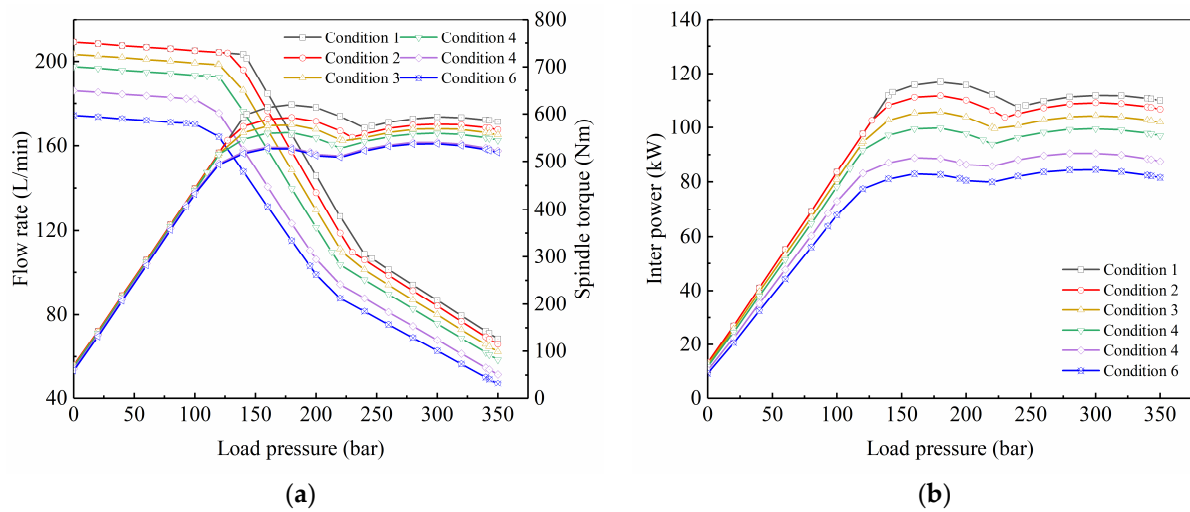


Figure 16. Constant power control curves of the double-compound axial piston pump under different working conditions: (a) outlet flow and spindle torque; (b) input power.

5.2. Analysis of Variable Power Control Characteristics

In order to realize the variable power control of the double-compound axial piston pump, the active control quantities are the rotational speed of the prime motor and the power control pilot pressure. The rated pressure of the double-compound axial piston pump is 343 bar, so it is representative to analyze the power control characteristics of the pump under the load pressure of 343 bar.

Figures 17 and 18 show the output flow, volumetric efficiency, output power, and overall efficiency of the double-compound axial piston pump when the load pressure is 343 bar. The outlet flow of the double-compound axial piston pump decreases with an increase in the power control pilot pressure, but increases with an increase in the rotational speed. The output power shows the same trend as the outlet flow, as shown in Figures 17a and 18a. The volumetric efficiency and overall efficiency of piston pump decrease with an increase in the power control pilot pressure, but increase with an increase in the rotational speed. In other words, the double-axial piston pump has higher output efficiency when the output flow is larger. The contour lines of the surface in Figures 17a and 18a indicate the same output flow and the same output power. Therefore, the accurate matching between the output flow and working rate of the hydraulic system can be achieved by comprehensively adjusting the power control pilot pressure and the rotational speed of the prime mover.

Figure 19 shows the spindle torque and input power of the double-compound axial piston pump under a 343 bar load pressure. Under the same load pressure, the spindle torque decreases with an increase in the power control pilot pressure, but increases with an increase in the rotational speed. Moreover, the input power shows the same trend as the spindle torque. The contour lines of the surface in figure indicate the same spindle torque and the same input power. When matching the characteristic curve of the piston pump and the engine, the surface diagram has important guiding significance.

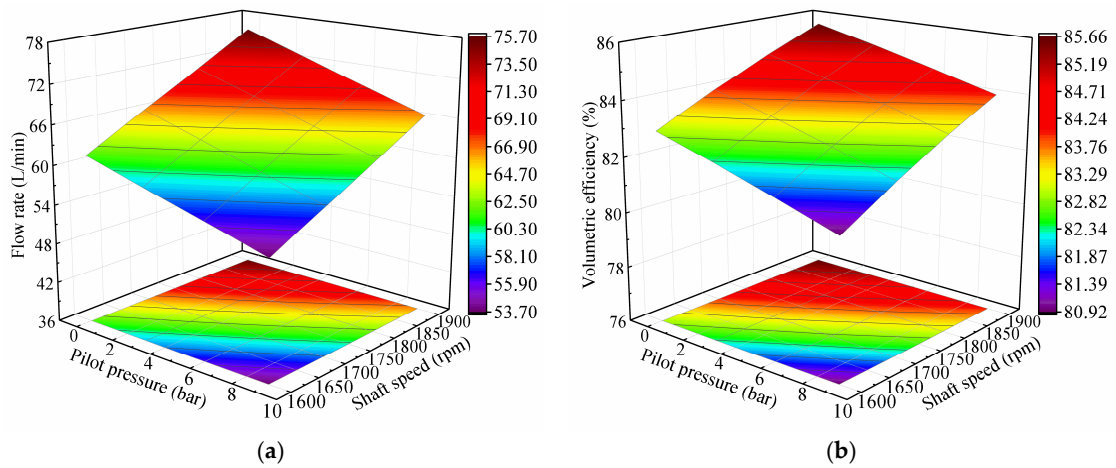


Figure 17. Output flow and volumetric efficiency of the double-compound axial piston pump: (a) outlet flow; (b) volumetric efficiency.

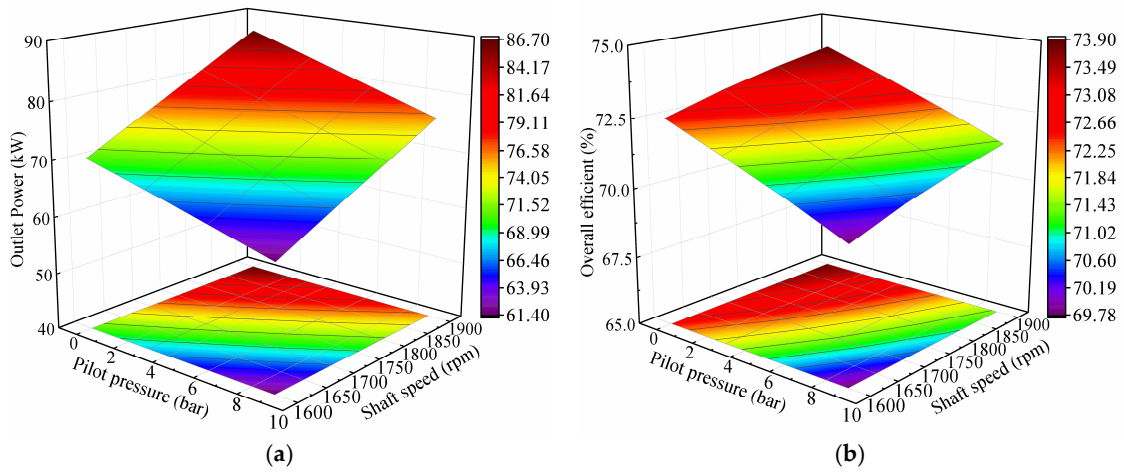


Figure 18. Output power and overall efficiency of the double-compound axial piston pump: (a) outlet power; (b) overall efficiency.

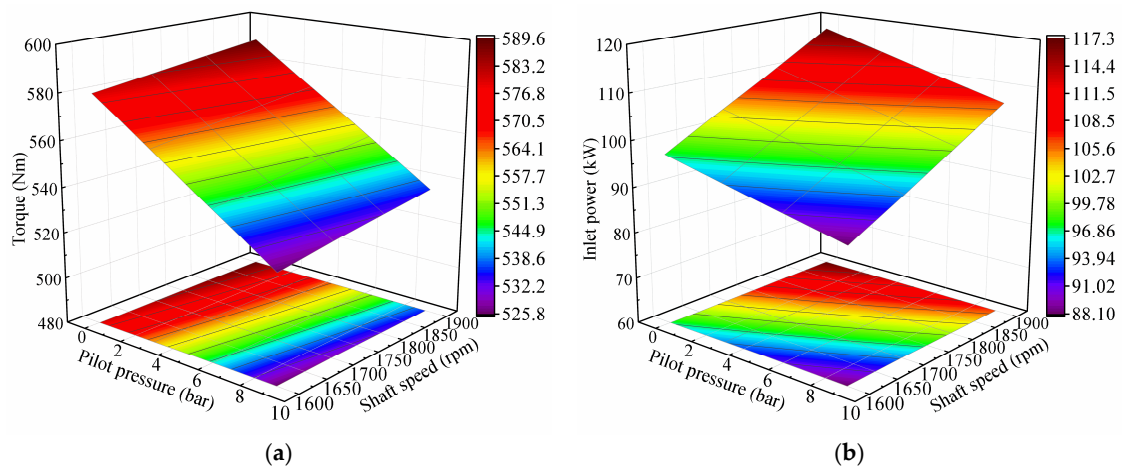


Figure 19. Spindle torque and input power of the double-compound axial piston pump: (a) spindle torque; (b) input power.

6. Dynamic Characteristics Analysis of the Double-Compound Axial Piston Pump

Taking a cycle under the load pressure of 343 bar as an example, the flow pulsation and pressure shock of a single piston chamber in a cycle are analyzed. The movement of the piston chamber is divided into eight stages, so there are eight critical positions, as shown in Figure 20. Figure 21 shows the dynamic characteristics of a single piston chamber in one cycle.

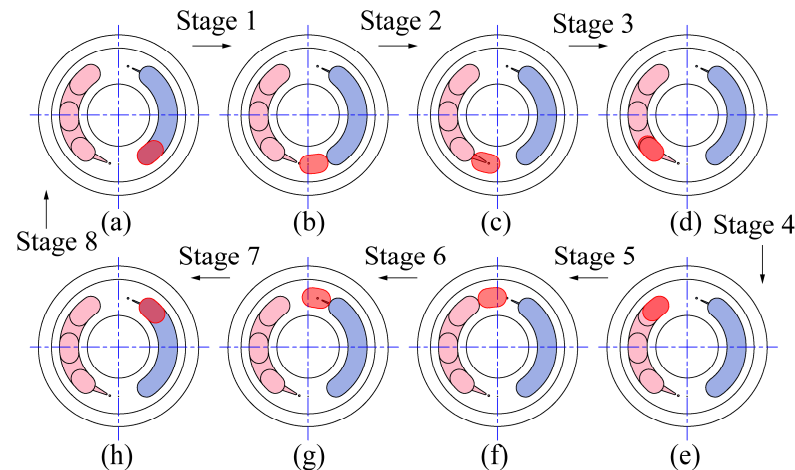


Figure 20. Working stages of the piston chamber: (a–h) critical positions between work stages.

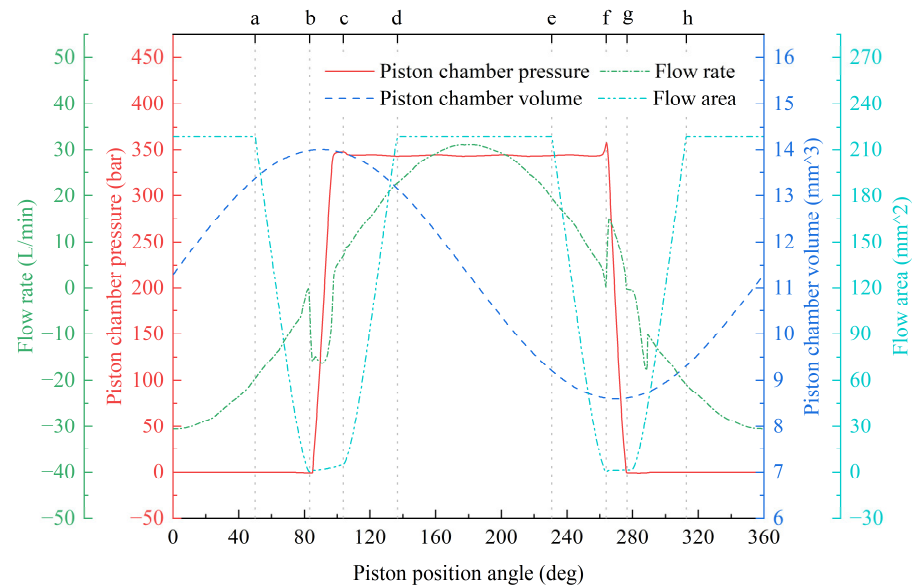


Figure 21. Dynamic characteristics of the piston chamber in one cycle. a–h are critical positions between work stages.

In stage 1, the piston chamber begins to separate from the oil suction area, the flow area of the piston chamber gradually decreases, and it is completely separated from the oil suction area at position b. In stage 2, the piston chamber enters the closed pre-compression pressure zone, and carries out mechanical expansion before crossing the top dead center. Starting from the top dead center, the volume is compressed by mechanical method. The piston chamber is connected to the high-pressure area through the damping hole and the triangular damping groove, and mechanical expansion occurs at the same time, resulting in the oil backflow from the high-pressure area to the piston chamber. In the initial stage, the pressure in the piston chamber is negatively overshoot due to mechanical expansion. The pre-compression pressure process ends at position c, and there is a positive pressure

overshoot at this position, which is mainly caused by mechanical compression and oil backflow. Due to oil backflow and pressure overshoot, oil hammer and noise occur in the piston pump. In stage 3, the flow area of the piston chamber increases rapidly, and the pressure of the piston chamber is rapidly balanced with the pressure of the oil discharge area. The piston chamber fully enters the oil discharge area at position d. In stage 4, the flow area of the piston chamber is constant. Because the volume change rate of the piston chamber first increases and then decreases, the instantaneous flow peak of oil discharge occurs in this stage. In stage 5, the piston chamber is gradually separated from the oil discharge area, and the flow area gradually decreases, while the volume of the piston chamber continues to decrease. When the flow area is too small, the mechanical compression occurs, the pressure of the piston chamber increases, and the pressure is positive overshoot. In stage 6, the piston chamber enters the closed pre-release pressure zone. The piston chamber is connected to the low-pressure area through the damping hole and the triangular damping groove, and the pressure of the piston chamber decreases rapidly to carry out the pre-release pressure of the piston chamber. When the piston chamber is connected to the low-pressure area, the oil backflow from the piston chamber to the low-pressure area occurs. In stage 7, in the initial stage, the flow area of the piston chamber is small, and the mechanical volume expansion occurs, resulting in negative pressure overshoot. The pressure overshoot is mainly caused by mechanical expansion and oil backflow. Then, the oil in the low-pressure area flows back to the piston chamber. In stage 8, the flow area of the piston chamber is constant. Since the volume change rate of the piston chamber first increases and then decreases, there is an instantaneous flow peak of oil suction in this stage.

Figure 22 shows the dynamic flow characteristics of the piston pump and nine piston chambers in one cycle. At the same time, four or five piston chambers are connected to the oil discharge area of the port plate, while the other piston chambers are disconnected from the oil discharge area of the port plate. A change in the number of piston chambers connected to the oil discharge area and the sinusoidal motion of the piston generate the structure flow pulsation of the piston pump. In addition, the oil backflow in the piston chamber can cause dynamic flow pulsation, especially the oil backflow in the closed pre-compression pressure zone, which is usually the main cause of the flow pulsation at the outlet of the piston pump, as shown in region A in the figure. Additionally, the number of outlet flow pulsations of the piston pump is the same as the number of piston chambers in a cycle.

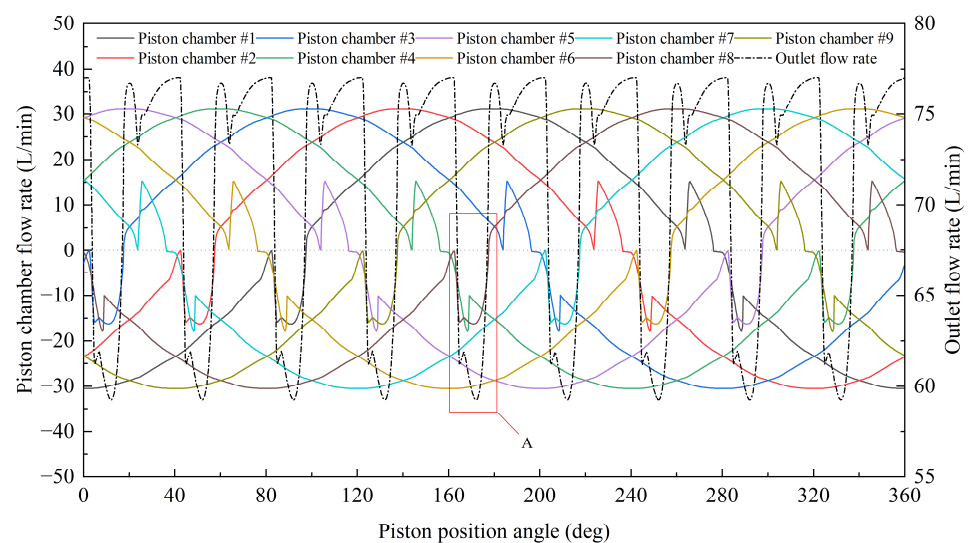


Figure 22. Dynamic flow characteristics of the piston pump and piston chambers in one cycle.

6.1. Influence of Load Pressure on Dynamic Characteristics

The same load pressure is set for the front pump and the rear pump to analyze the influence of different load pressures on the dynamic characteristics of the piston pump. The spindle speed is 1800 rpm; the power control pilot pressure is 0 bar; and the load pressure is 70, 143, 200, 246, 300, and 343 bar, respectively.

Taking the front pump as an example, the outlet flow and the pulsation rate of the piston pump are shown in Figure 23. Since the double-compound axial piston pump adopts the power control mode in the working state, before the power setting starting point, the inclination angle of the swash plate is the largest, and the piston pump operates with largest flow rate. The flow rate of the piston pump is basically unchanged. After the power setting starting point, the flow rate of the piston pump decreases with an increase in the load pressure. Due to the same spindle speed, the piston pump has the same frequency under different load pressures, so the frequency of flow pulsation is also the same. The pulsation range of the outlet flow of the piston pump changes little with load pressure, while the flow pulsation rate increases with load pressure, as shown in Figure 23b. Therefore, the load pressure has a great influence on the flow pulsation of the piston pump.

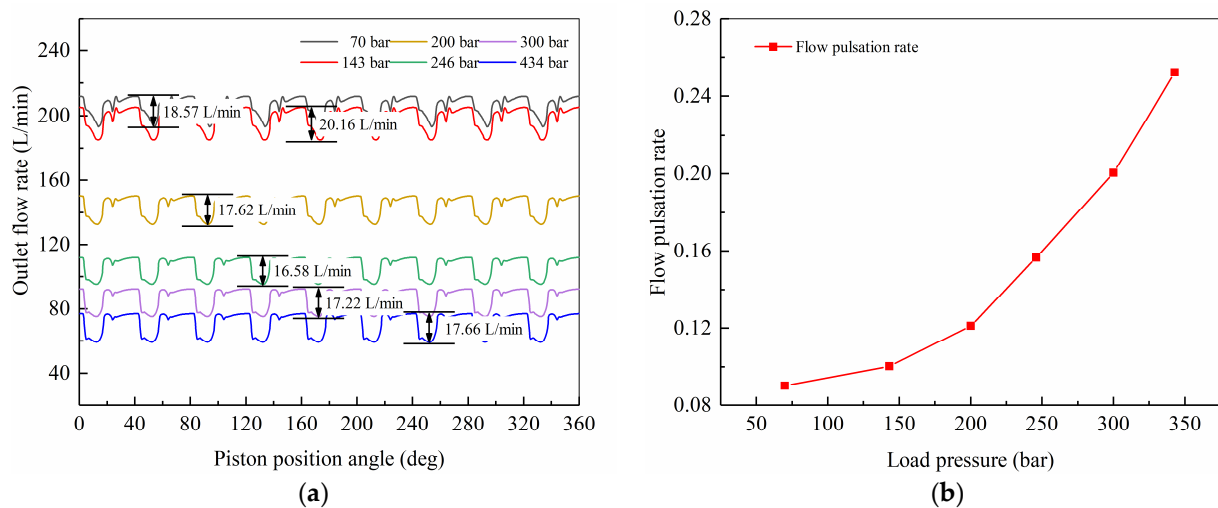


Figure 23. Outlet flow pulsation and pulsation rate under different load pressures: (a) outlet flow; (b) flow pulsation rate.

Figure 24 shows the variation of dynamic flow and pressure of the piston chamber with load pressure in one cycle. At this time, the power starting pressure of the piston pump is 143 bar. Before the starting pressure, the dynamic flow of the piston chamber decreases slightly with an increase in the load pressure, which is mainly caused by leakage. After the starting pressure, the instantaneous flow rate of the piston chamber also decreases with an increase in the load pressure because the inclination angle of the swash plate decreases with an increase in the load pressure. The oil backflow in the closed pre-compression pressure zone still exists even under a low load pressure, and the backflow flow increases with an increase in the load pressure. When the piston chamber begins to discharge oil to the high-pressure zone, namely at the position c, the discharge flow shows a peak-shaped mutation, and the mutation discharge flow decreases with an increase in the load pressure. The oil backflow in the closed pre-release pressure zone exists under low and high load pressures, and the backflow flow increases with an increase in the load pressure. When the piston chamber starts to suck oil from the low-pressure area, i.e., when the piston position angle is 285 deg, there is a wedge-shaped mutation in the waveform of oil suction flow, and the mutation value of oil suction flow decreases with an increase in the load pressure.

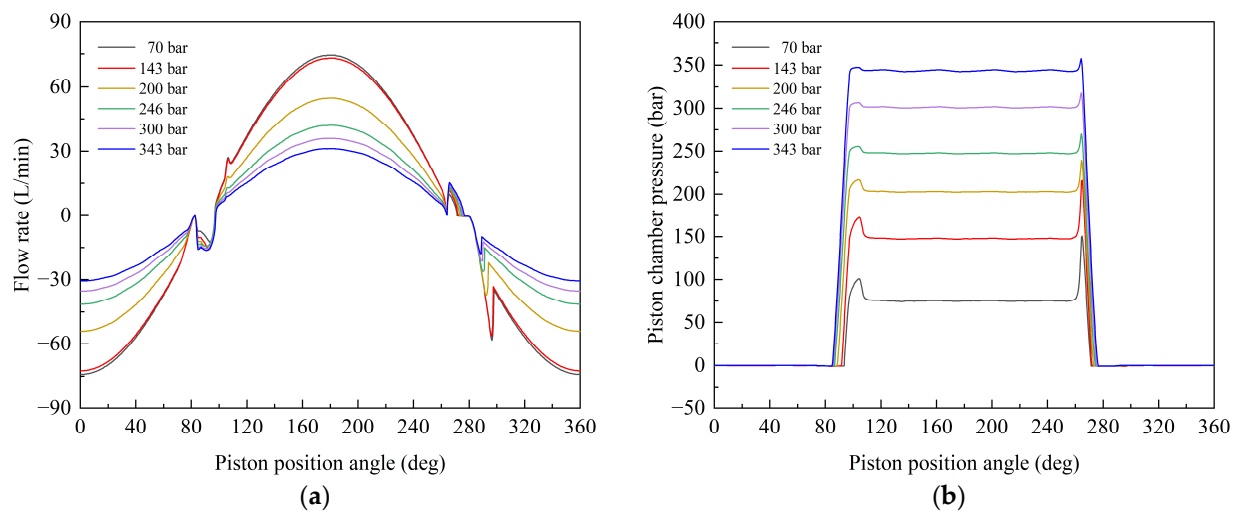


Figure 24. Flow and pressure characteristics of the piston chamber under different load pressures: (a) dynamic flow; (b) dynamic pressure.

The positive pressure overshoot of the piston chamber at position c decreases with an increase in the load pressure, and the positive pressure overshoot at position f decreases with an increase in the load pressure. The position angle which the pressure of low-pressure piston chamber begins to rise decrease with an increase in the load pressure, while the position angle of the piston chamber falling from high pressure to low pressure increases with an increase in the load pressure.

The internal leakage of the axial piston pump is mainly composed of three parts: port plate–barrel block pair leakage, slipper–swash plate pair leakage, and piston–barrel block pair leakage. Figure 25 shows the variation of leakage flow of the piston pump and kinematic pairs with load pressure. Under a constant load pressure, the leakage flow fluctuation of the piston pump is small, and the leakage flow rate is basically constant. By comparing the leakage flow of kinematic pairs, it is found that the leakage flow of the piston pump mostly comes from the leakage of the port plate–barrel block pair. There is a linear positive correlation between leakage flow of the port plate–barrel block pair of the piston pump and load pressure. The change trend of leakage flow of the slipper–swash plate pair is the same as that of piston chamber pressure. The leakage flow of the piston–barrel block pair is not only related to the pressure of the piston chamber, but also to the axial velocity of the piston. Therefore, the leakage flow of the piston pump is basically linearly positively correlated with the load pressure.

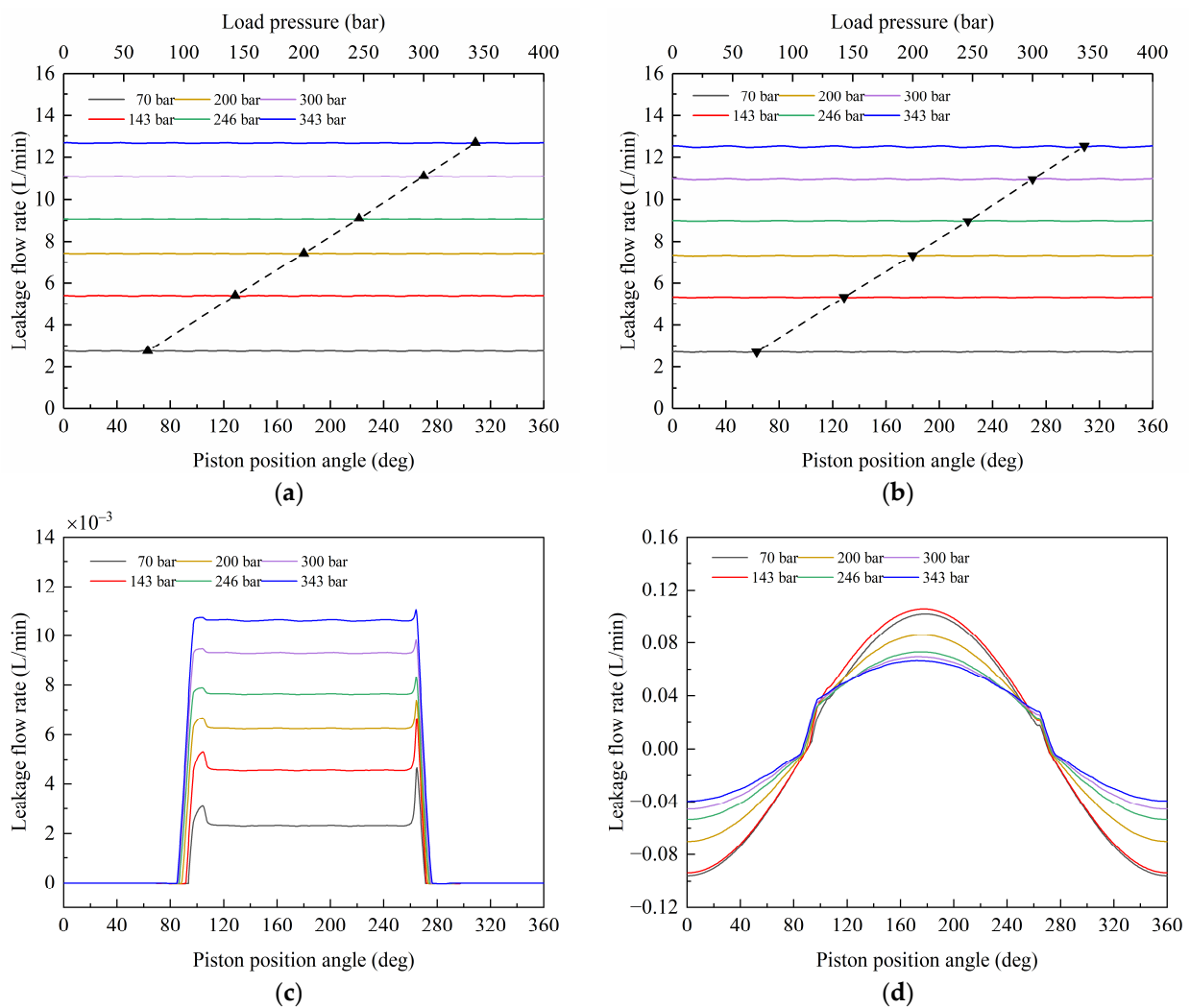


Figure 25. Leakage flow of the piston pump and kinematic pairs under different load pressures: (a) leakage flow rate of the piston pump; (b) leakage flow rate of the port plate-barrel block pair; (c) leakage flow rate of the slipper-swash plate pair; (d) leakage flow rate of the piston-barrel block pair.

6.2. Influence of Spindle Speed on Dynamic Characteristics

The front pump and rear pump are set with the same load pressure, and the influence of different spindle speed on the dynamic characteristics of the piston pump is analyzed. The load pressure is 343 bar; the power control pilot pressure is 0.0 bar; and the spindle speed is 1500, 1600, 1700, 1800, 1900, and 2000 rpm, respectively.

For the front pump, for example, the outlet flow and pulsation rate of the piston pump are shown in Figure 26. Under the same load pressure and power control pilot pressure, with an increase in the spindle speed, the outlet flow increases and the flow pulsation frequency increases. The flow pulsation range of the outlet flow of the piston pump increases with an increase in the spindle speed, but the flow pulsation rate decreases with an increase in the spindle speed, as shown in Figure 26b. Therefore, increasing the spindle speed of the piston pump can effectively reduce the outlet flow pulsation.

Figure 27 shows the variation of dynamic flow and pressure of the piston chamber with spindle speed in one cycle. Since the load pressure is greater than the power starting pressure, the piston pump operates at a small displacement. The oil backflow flow in the closed pre-compression pressure zone increases with an increase in the spindle speed. At position c, the discharge flow mutation is not obvious. The change in spindle speed has little effect on the oil backflow in the closed pre-release pressure zone. When the piston

chamber begins to suck oil from the low-pressure area, i.e., when the piston position angle is 285 deg, there is a wedge-shaped mutation in the waveform of oil suction flow, and the mutation value of oil suction flow increases with an increase in the spindle speed.

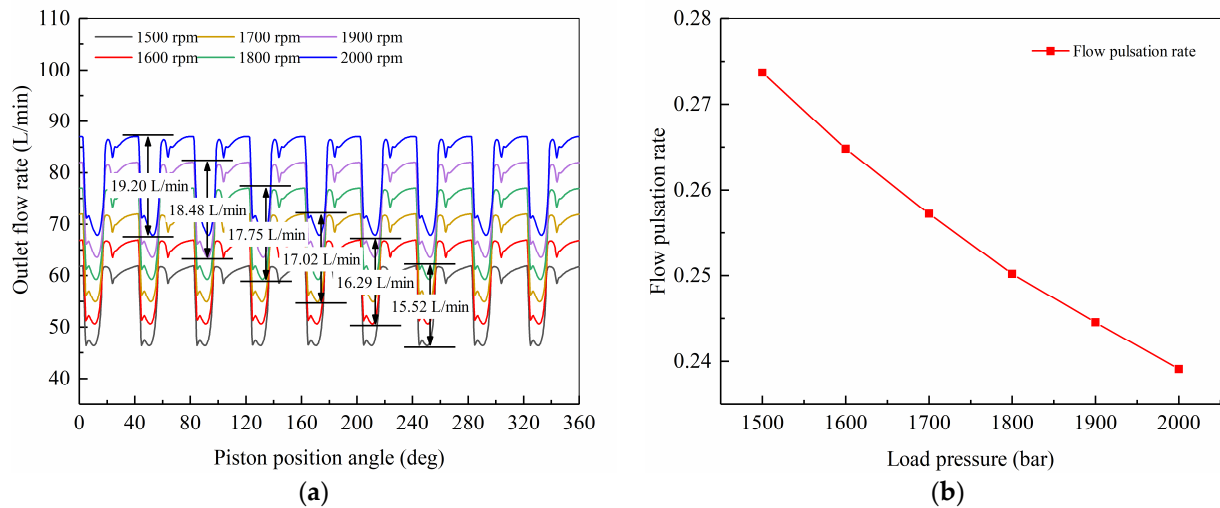


Figure 26. Outlet flow pulsation and pulsation rate under different spindle speeds: (a) outlet flow; (b) flow pulsation rate.

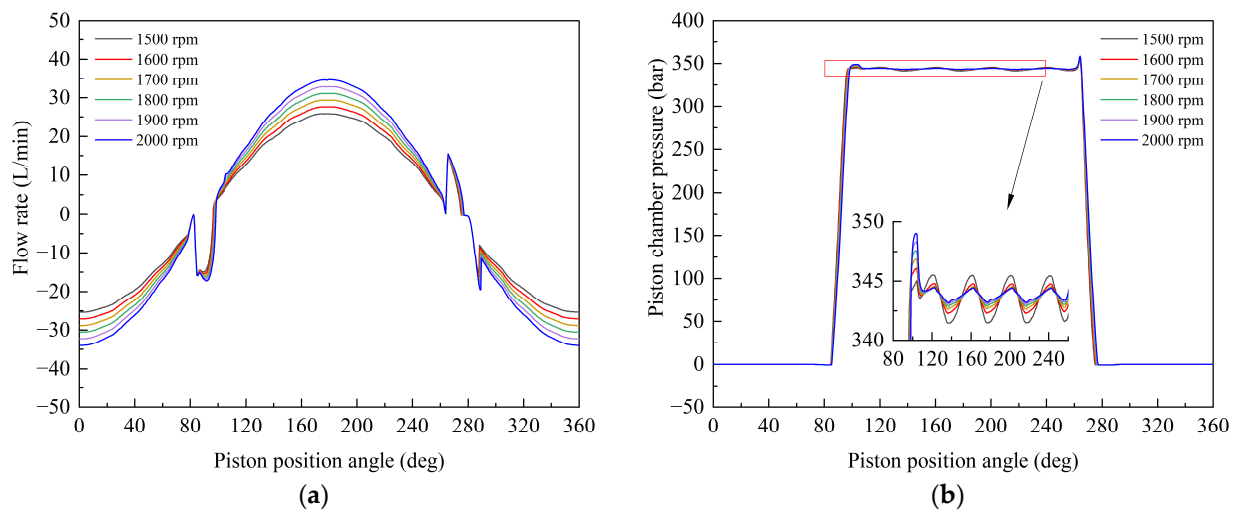


Figure 27. Flow and pressure characteristics of the piston chamber under different spindle speeds: (a) dynamic flow; (b) dynamic pressure.

The pressure overshoot of the piston chamber at position c increases slightly with an increase in the spindle speed. The position angle of the pressure of low-pressure piston chamber begins to rise, which is not obviously affected by the spindle speed, while the position angle of the piston chamber falling from high pressure to low pressure increases slightly with an increase in the spindle speed. When the piston chamber is in the oil discharge area, the pressure in the chamber fluctuates slightly. The pressure pulsation frequency increases with an increase in the spindle speed, while the amplitude of pressure decreases with an increase in the spindle speed.

Figure 28 shows the variation of leakage flow of the piston pump and kinematic pairs with spindle speed. Under the same load pressure, the leakage flow of the piston pump presents a small pulsation. The leakage pulsation frequency increases with an increase in the spindle speed, but the pulsation amplitude decreases with an increase in the spindle speed. The leakage flow of the piston pump increases slightly with an increase in the

spindle speed. The leakage flow of the port plate–barrel block pair also presents a small pulsation. The pulsation frequency increases with an increase in the spindle speed, while the pulsation amplitude decreases with an increase in the spindle speed. The influence of the spindle speed on the leakage flow rate of the port plate–barrel block pair is small. The change trend of leakage flow in the slipper–swash plate pair is the same as that of piston chamber pressure. The leakage flow of the piston–barrel block pair increases with an increase in the spindle speed. Therefore, increasing the spindle speed can effectively reduce the leakage flow pulsation of the piston pump.

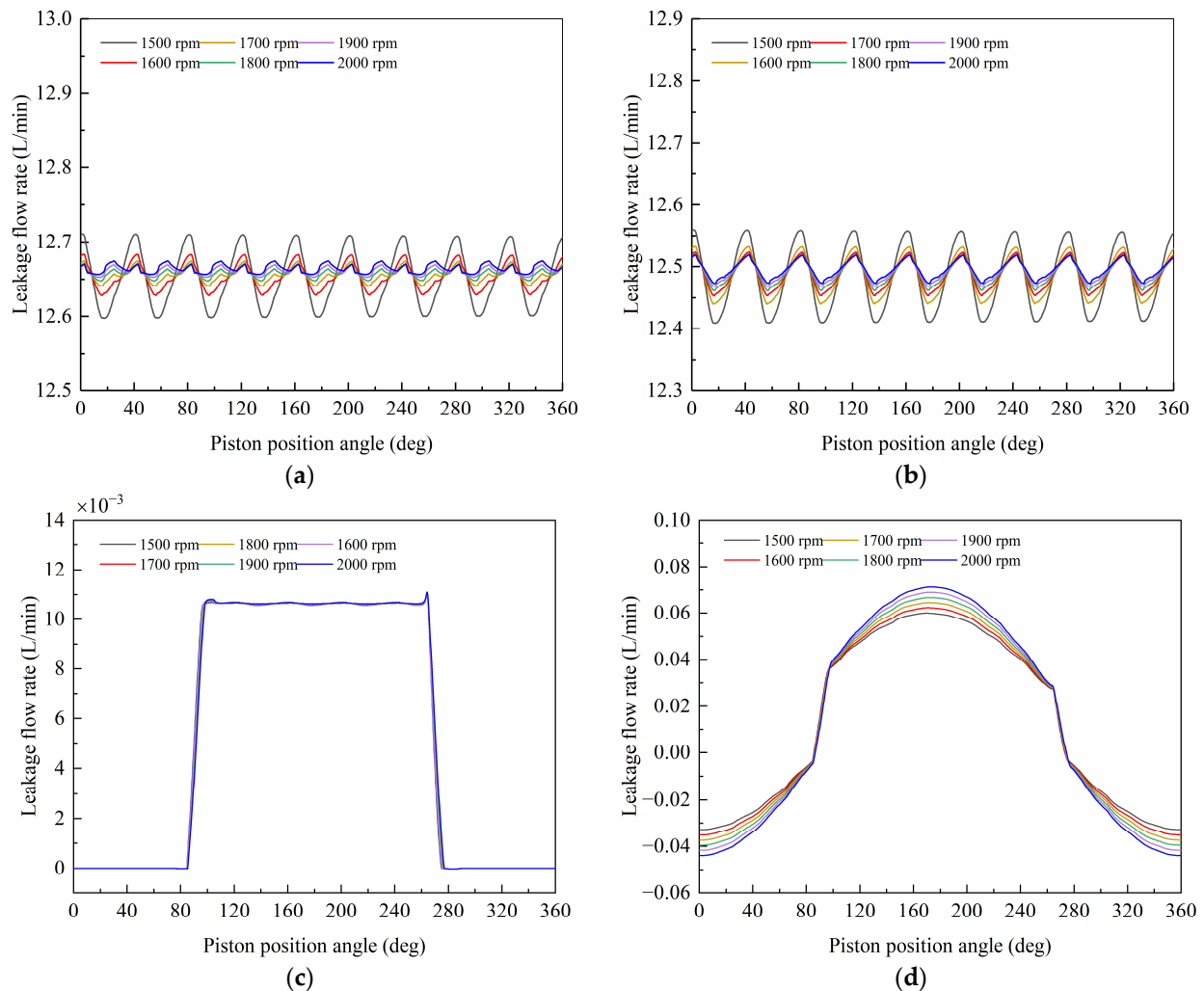


Figure 28. Leakage flow of the piston pump and kinematic pairs under different spindle speeds: (a) leakage flow rate of the piston pump; (b) leakage flow rate of the port plate–barrel block pair; (c) leakage flow rate of the slipper–swash plate pair; (d) leakage flow rate of the piston–barrel block pair.

6.3. Influence of Power Control Pilot Pressure on Dynamic Characteristics

The same load pressure is set for the front pump and the rear pump, and the influence of different power control pilot pressure on the dynamic characteristics of the piston pump is analyzed. The load pressure is 343 bar; the spindle speed is 1800 rpm; and the power control pilot pressure is 0.0, 1.5, 3.0, 4.5, 6.0, and 7.5 bar, respectively.

The outlet flow and pulsation rate of the piston pump are shown in Figure 29. Under the same load pressure and spindle speed, the outlet flow decreases with an increase in the power control pilot pressure. The flow pulsation range of the outlet flow of the piston pump decreases with an increase in the power control pilot pressure, but the flow pulsation

rate increases with an increase in the pilot pressure, as shown in Figure 29b. Therefore, an increase in the power control pilot pressure can aggravate the outlet flow pulsation of the piston pump.

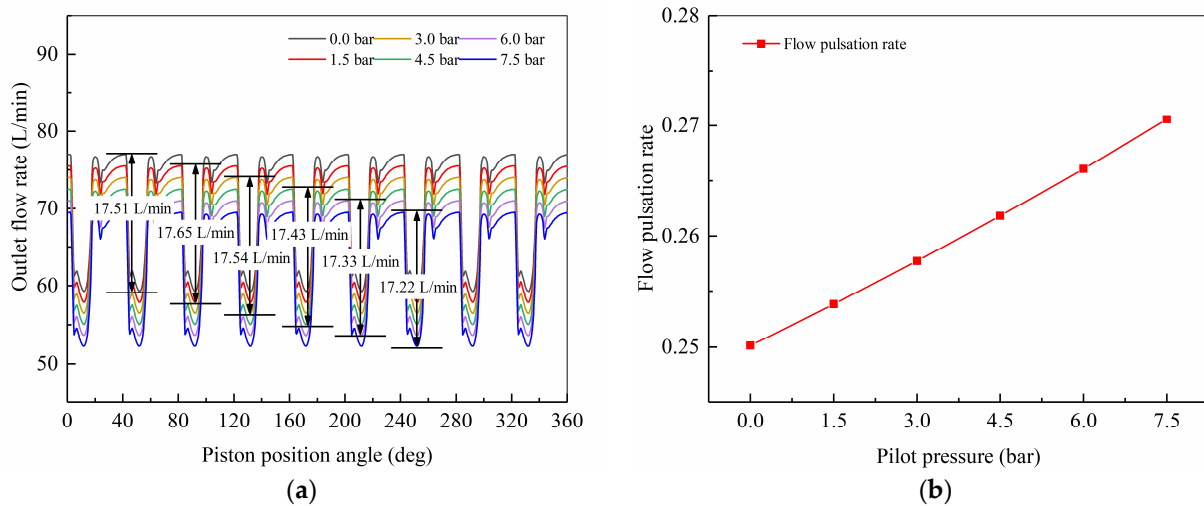


Figure 29. Outlet flow pulsation and pulsation rate under different power control pilot pressures: (a) outlet flow; (b) flow pulsation rate.

Figure 30 shows the variation of dynamic flow and pressure of the piston chamber with power control pilot pressure. Since the load pressure is greater than the power starting pressure, the piston pump operates at a small displacement. The oil backflow in the closed pre-compression pressure zone and the closed pre-release pressure zone is less affected by the power control pilot pressure. Furthermore, at position c, the mutation of oil discharge flow is not obvious. When the piston chamber starts to suck oil from the low-pressure area, i.e., when the piston position angle is 285 deg, the mutation value of the oil suction flow decreases slightly with an increase in the pilot pressure. The power control pilot pressure has little effect on the dynamic pressure in the piston chamber, as shown in Figure 30b.

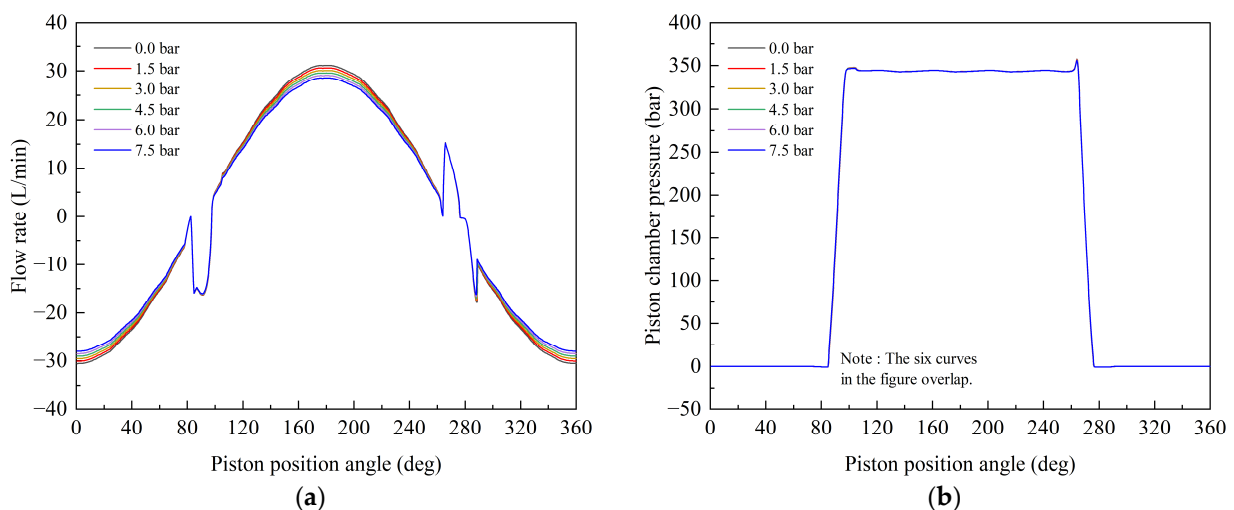


Figure 30. Flow and pressure characteristics of the piston chamber under different power control pilot pressures: (a) dynamic flow; (b) dynamic pressure.

Figure 31 shows the variation of leakage flow of the piston pump and kinematic pairs with power control pilot pressure. Under the same load pressure and spindle speed, the leakage flow of the piston pump presents small pulsation. The leakage flow pulsation frequency under different pilot pressure is the same. The pulsation amplitude increases

with an increase in the pilot pressure, and the leakage flow of the piston pump decreases slightly with an increase in the pilot pressure. The leakage flow of the port plate–barrel block pair also presents small pulsation. The leakage pulsation frequency of the port plate–barrel block pair under different pilot pressures is the same. The pulsation amplitude increases slightly with an increase in the pilot pressure, but the leakage flow of the port plate–barrel block pair decreases slightly with an increase in the pilot pressure. The leakage flow change trend of the slipper–swash plate pair is the same as that of the piston chamber pressure, which is less affected by pilot pressure. The leakage flow of the piston–barrel block pair decreases with an increase in the pilot pressure.

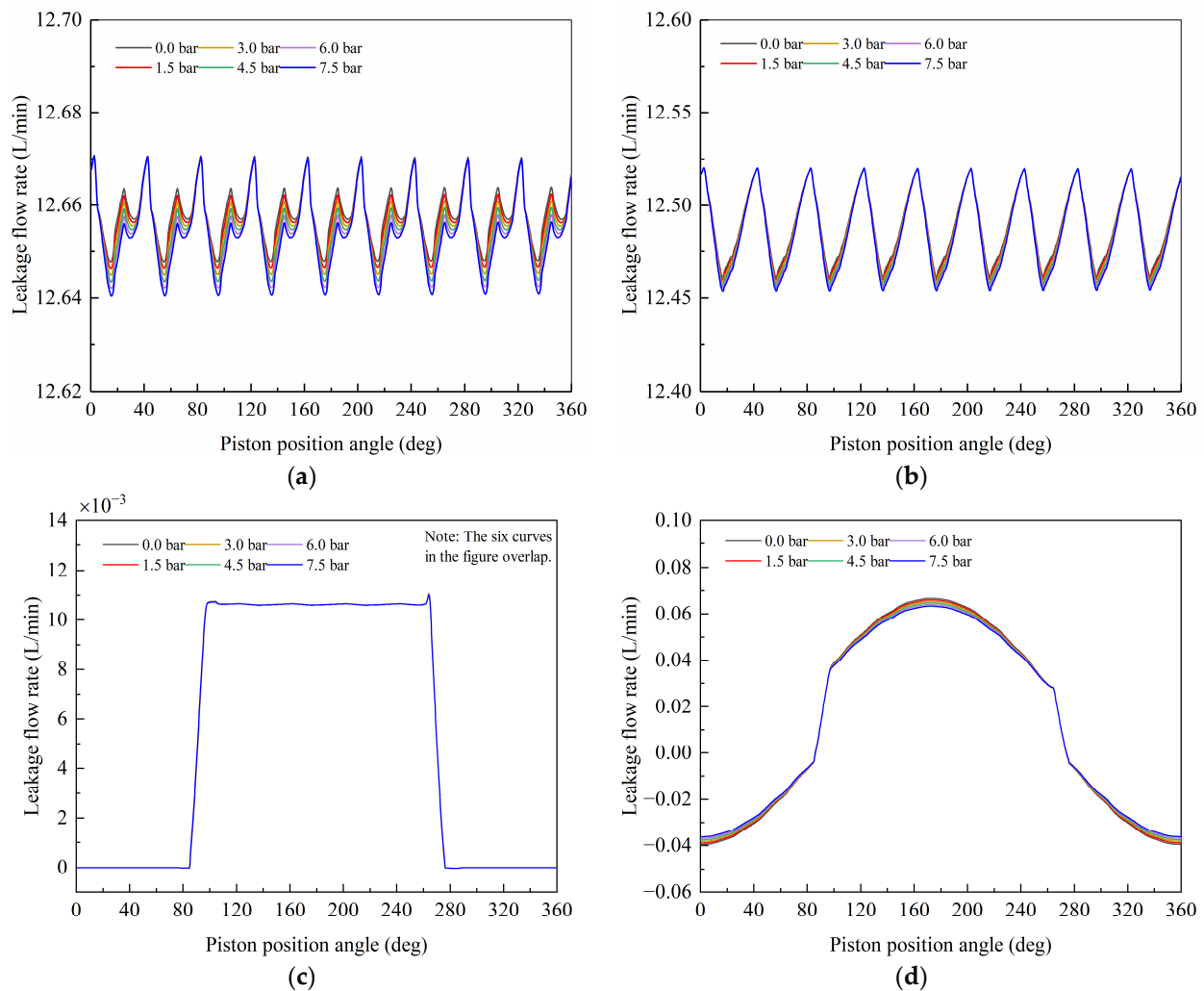


Figure 31. Leakage flow of the piston pump and kinematic pairs under different power control pilot pressures: (a) leakage flow rate of the piston pump; (b) leakage flow rate of the port plate–barrel block pair; (c) leakage flow rate of the slipper–swash plate pair; (d) leakage flow rate of the piston–barrel block pair.

7. Conclusions

In this paper, by analyzing the working and control principle of the double-compound axial piston pump, the numerical model of the double-compound axial piston pump is established. In this model, the leakage of the slipper–swash plate pair and the piston–barrel block pair is thought to come from the piston chamber, while the leakage of the port plate–barrel block pair is thought to come from the oil suction chamber and the oil discharge chamber. Numerical simulation and experimental tests are carried out under the same working conditions. The results show that the simulation results and experimental

results show the same trend, and the numerical simulation results are in good agreement with the experimental results, and the error is within the allowable range. The established numerical model of the double-compound axial piston pump can effectively analyze the control and dynamic characteristics of the double-compound axial piston pump. Moreover, compared with the traditional practical experiments, the numerical method is more efficient, convenient, and cost-effective in the design stage.

Under various working conditions, the constant power and variable power control characteristics of the double-compound axial piston pump are analyzed. The results show that under the power control mode, the power control pilot pressure controls the left and right movement of the flow curve, while the spindle speed controls the up-and-down movement of the flow curve. Under the rated load pressure, the output efficiency of the double-compound axial piston pump is higher when the output flow is larger. The accurate matching of the output flow and working rate of the double-compound axial piston pump, input power, and power characteristics of prime mover can be realized by comprehensively adjusting the power control pilot pressure and the rotational speed of prime mover.

The influence laws of different working conditions on the dynamic flow and pressure characteristics of the double-compound axial piston pump are clarified by analyzing the dynamic characteristics of the double-compound axial piston pump. When the piston chamber works in the closed pre-compression pressure zone, the oil in the high-pressure area flows back to the piston chamber, and the backflow flow increases with an increase in the load pressure and spindle speed, which is less affected by the power control pilot pressure. When the piston chamber works in the closed pre-release pressure zone, the oil backflow from the piston chamber to the low-pressure area occurs, and the backflow flow increases with an increase in the load pressure, which is less affected by the spindle speed and power control pilot pressure. The oil backflow of the piston chamber is the main reason for the outlet flow pulsation of the double-compound axial piston pump. An increase in load pressure and power control pilot pressure can aggravate the outlet flow pulsation, while increasing the spindle speed can effectively reduce the outlet flow pulsation.

Although this work obtained some research results, there are still some deficiencies. Due to the limitations of the experimental test and the difficulties associated with the flow pulsation test, the outlet flow pulsation has not been accurately tested. These need to be further refined in future research. In addition, for further research, it is also our main job to propose methods that can reduce flow pulsation on the basis of this study.

Author Contributions: Conceptualization, Z.S.; methodology, Z.S.; software, Z.S.; validation, Z.S., Q.Z. and L.W.; formal analysis, Z.S.; investigation, Z.S. and L.W.; Resources, H.D.; data curation, Z.S.; writing—original draft preparation, Z.S.; writing—review and editing, Q.Z. and Z.S.; visualization, Z.S.; supervision, Q.Z.; project administration, L.W.; funding acquisition, Q.Z. and L.W. All authors have read and agreed to the published version of the manuscript.

Funding: This research was funded by the National Natural Science Foundation of China (grant numbers: 51974170 and 52174146), the Natural Science Fund of Shandong Province (grant numbers: ZR2019MEE067 and ZR2019BEE066), and the Shandong Province Key Research and Development Program (grant number: 2019SDZY01).

Institutional Review Board Statement: Not applicable.

Informed Consent Statement: Not applicable.

Data Availability Statement: The data used to support the findings of this study are included within the article.

Conflicts of Interest: The authors declare no conflict of interest.

Nomenclature

A_d, A_x	action area of large cavity and action area of small cavity of the actuator piston (m ²)
A_f	effective area of the power control pilot pressure acting on the power control valve (m ²)
A_{ncv}	effective area of the pilot control pressure acting on the negative flow control valve (m ²)
A_{pcv1}, A_{pcv2}	effective area of load pressure of the front/rear pump acting on power control valve (m ²)
$A_{pin,i}, A_{pout,i}$	flow area between the inlet/outlet main groove and the <i>i</i> th piston chamber (m ²)
c_{ap}	damping coefficient of the actuator piston (N/(m/s))
c_{ncv}	damping coefficient of the negative flow control valve (N/(m/s))
c_{pcv}	damping coefficient of the power control valve (N/(m/s))
c_{sp}	damping coefficient of the swash plate (N/(m/s))
c_{sv}	damping coefficient of the servo valve (N/(m/s))
C_d	flow coefficient
d_p	piston diameter (m)
d_{tp}	diameter of the piston damping orifice (m)
E	bulk modulus of the hydraulic oil (MPa)
e_p	eccentricity distance between the piston and the piston chamber (m)
F_{ncv0}	spring preload of the negative flow control valve (N)
$F_{p,i}$	equivalent force of the oil pressure on piston (N)
F_{pcv0}	spring preload of the power control valve (N)
$F_{pty,i}, F_{ptz,i}$	projections of the resultant force $F_{pt,i}$ on the <i>z</i> and <i>y</i> axis (N)
F_{sp}	force of the swash plate on the actuator piston (N)
F_{sv0}	spring preload of the servo valve (N)
$F_{vlpc,i}$	viscous friction caused by leakage of the piston–barrel block pair (N)
$F_{vlsy,i}, F_{vlsz,i}$	projections of the resultant force $F_{vls,i}$ on the <i>z</i> and <i>y</i> axis (N)
h_p	diameter gap between the piston and the piston chamber (m)
h_{ppb}	gap between the barrel block and the port plate (m)
h_{ssp}	gap between the slipper and the swash plate (m)
J_1	moment of inertia of the power control link around O_1 (kg·m ²)
J_2	moment of inertia of the negative flow control link around O_2 (kg·m ²)
J_{f4}, J_{f7}	moment of inertia of feedback fork around O_4/O_7 (kg·m ²)
J_{sp}	moment of inertia of the swash plate (kg·m ²)
k_1, k_2	spring stiffness of the outer–inner spring of the power control valve (N/m)
k_{ncv}	spring stiffness of the negative flow control valve (N/m)
k_{pcv}	spring stiffness of power control valve (N/m)
k_{sv}	spring stiffness of servo valve (N/m)
$l_{pc,i}$	contact length between the piston and the piston chamber (m)
L_{sp}	acting force arm of the actuator piston to the swash plate (m)
l_{tp}	length of piston damping orifice (m)
m_{ap}	mass of the actuator piston (kg)
m_{ncv}	mass of the negative flow control valve core (kg)
m_{pcv}	mass of the power control valve core (kg)
m_{sv}	mass of the servo valve core (kg)
p_{ap}	pressure of the large cavity of the actuator piston (MPa)
p_c	pressure of leakage cavity (MPa)
p_d	pump outlet pressure (MPa)
p_f	power control pilot pressure (MPa)
P_{vap}^H, P_{vap}^L	high/low-saturation vapor pressure (MPa)
p_{ncv}	negative flow control pilot pressure (MPa)
$p_{p,i}$	pressure of piston chamber (MPa)
p_s	pump inlet pressure (MPa)

P_{sat}	saturation pressure (MPa)
Q_l	total leakage flow (L/min)
$Q_{lpbb,i}$	leakage flow of the piston–barrel block pair (L/min)
Q_{lppb}	leakage flow of the port plate–barrel block pair (L/min)
$Q_{lssp,i}$	leakage flow of the slipper–swash plate pair (L/min)
$Q_{pin,i}, Q_{pout,i}$	inlet/outlet flow of piston chamber (L/min)
R	piston distribution radius (m)
r_{ext1}, r_{ext2}	inner/outer radius of the external port plate (m)
r_{int1}, r_{int2}	outer/inner radius of the internal port plate (m)
r_{spi}, r_{spo}	inner/outer radius of the slipper (m)
T_{sf}	spindle torque of piston pump (N·m)
T_{sp}	torque applied by the piston to the swash plate (N·m)
T_{vlpp}	viscous friction torque between the port plate and the barrel block (N·m)
$u_{p,i}$	Couette effect of the piston speed on the leakage flow (m/s)
V_0	structure dead volume of the piston chamber (m ³)
V_{ap}	volume of the large cavity of the actuator piston (m ³)
$V_{p,i}$	volume of piston chamber (m ³)
ω	rotational speed of the spindle (rad/s)
w_{sv}	flow area of the servo valve (m ²)
x_0	distance difference between zero position of double springs of the power control valve (m)
x_{ap}	displacement of the actuator piston (m)
x_{cvf}	feedback displacement of the servo valve (m)
x_{lim}	maximum displacement of the power control valve core (m)
x_{pcv}	displacement of the power control valve core (m)
x_{sv}	displacement of the servo valve (m)
$y_{p,i}$	force arm of the resultant force along the z axis in the y direction (m)
$z_{p,i}$	force arm of the resultant force along the y axis in the z direction (m)
β	inclination angle of the port plate (rad)
$\theta_{in}, \theta_{out}$	angle range of the inlet/outlet main groove of the port plate (rad)
μ	dynamic viscosity (kg/m·s)
$\mu_{p,i}$	dynamic viscosity of the piston–barrel block pair gap (kg/m·s)

References

- Jong, K.; Jae, Y. Measurement of Fluid film thickness on the Valve Plate in Oil Hydraulic Axial Piston Pumps (I)—Bearing Pad Effects. *J. Mech. Sci. Technol.* **2003**, *17*, 246–253.
- Kim, J.-K.; Kim, H.-E.; Lee, Y.-B.; Youn, J.J.; Oh, S.-H. Measurement of Fluid Film Thickness on The Valve Plate in Oil Hydraulic Axial Piston Pumps (Part II Spherical Design Effects). *J. Mech. Sci. Technol.* **2005**, *19*, 655–663. [[CrossRef](#)]
- Cho, I.S.; Jung, J. A study on the pressure ripple characteristics in a bent-axis type oil hydraulic piston pump. *J. Mech. Sci. Technol.* **2013**, *27*, 3713–3719. [[CrossRef](#)]
- Cho, I.S. A study on the optimum design for the valve plate of a swash plate-type oil hydraulic piston pump. *J. Mech. Sci. Technol.* **2015**, *29*, 2409–2413. [[CrossRef](#)]
- Shin, J.H. Computational study on dynamic pressure in a swash-plate axial piston pump connected to a hydraulic line with an end resistance. *J. Mech. Sci. Technol.* **2015**, *29*, 2381–2390. [[CrossRef](#)]
- Stosiak, M. The impact of hydraulic systems on the human being and the environment. *J. Theor. Appl. Mech.* **2015**, *53*, 409–420. [[CrossRef](#)]
- Kudzma, Z.; Stosiak, M. Reduction of infrasounds in machines with hydrostatic drive. *Acta Bioeng. Biomech.* **2013**, *15*, 51–64. [[CrossRef](#)]
- Kim, J.-K.; Kim, H.-E.; Youn, J.J.; Oh, S.-H.; Jung, S.-H. Relation between Pressure Variations and Noise in Axial Type Oil Piston Pumps. *J. Mech. Sci. Technol.* **2004**, *18*, 1019–1025. [[CrossRef](#)]
- Edge, K.A.; Darling, J. The Pumping Dynamics of Swash Plate Piston Pumps. *J. Dyn. Syst. Meas. Control* **1989**, *111*, 307–312. [[CrossRef](#)]
- Manring, N.D. The Discharge Flow Ripple of an Axial-Piston Swash-Plate Type Hydrostatic Pump. *J. Dyn. Syst. Meas. Control* **2000**, *122*, 263–268. [[CrossRef](#)]
- Manring, N.D.; Dantew, F.A. The Control Torque on the Swash Plate of an Axial-Piston Pump Utilizing Piston-Bore Springs. *J. Dyn. Syst. Meas. Control* **2001**, *123*, 471–478. [[CrossRef](#)]
- Manring, N.D.; Zhang, Y. The Improved Volumetric-Efficiency of an Axial-Piston Pump Utilizing a Trapped-Volume Design. *J. Dyn. Syst. Meas. Control* **2001**, *123*, 479–487. [[CrossRef](#)]

13. Mandal, N.P.; Saha, R.; Sanyal, D. Theoretical simulation of ripples for different leading-side groove volumes on manifolds in fixed-displacement axial-piston pump. *Proc. Inst. Mech. Eng. Part I J. Syst. Control Eng.* **2008**, *222*, 557–570. [[CrossRef](#)]
14. Bergada, J.M.; Watton, J.; Kumar, S. Pressure, flow, force, and torque between the barrel and port plate in an axial piston pump. *J. Dyn. Syst. Meas. Control.* **2008**, *130*, 16. [[CrossRef](#)]
15. Tong, S.; Wang, X.; Zhong, W.; Zhang, J. Dynamic characteristics analysis on axial piston pump based on virtual prototype technology. *J. Mech. Eng.* **2013**, *49*, 174–182. [[CrossRef](#)]
16. Bergada, J.M.; Kumar, S.; Davies, D.L.; Watton, J. A complete analysis of axial piston pump leakage and output flow ripples. *Appl. Math. Model.* **2012**, *36*, 1731–1751. [[CrossRef](#)]
17. Fu, Y.; Yang, J.; Zhu, D.; Destech Publicat, I. Analysis of Dynamic and Static Performance of Axial Plunger Electro-hydraulic Pump. In Proceedings of the 2016 3rd International Conference on Mechanical, Industrial, and Manufacturing Engineering, Los Angeles, CA, USA, 30–31 January 2016; pp. 150–156.
18. Xu, B.; Ye, S.G.; Zhang, J.H.; Zhang, C.F. Flow ripple reduction of an axial piston pump by a combination of cross-angle and pressure relief grooves: Analysis and optimization. *J. Mech. Sci. Technol.* **2016**, *30*, 2531–2545. [[CrossRef](#)]
19. Casoli, P.; Vacca, A.; Franzoni, G.; Berta, G.L. Modelling of fluid properties in hydraulic positive displacement machines. *Simul. Model. Pract. Theory* **2006**, *14*, 1059–1072. [[CrossRef](#)]
20. Ye, S.G.; Zhang, J.H.; Xu, B. Noise Reduction of an Axial Piston Pump by Valve Plate Optimization. *Chin. J. Mech. Eng.* **2018**, *31*, 16. [[CrossRef](#)]
21. Ouyang, X.P.; Fang, X.; Yang, H.Y. An investigation into the swash plate vibration and pressure pulsation of piston pumps based on full fluid-structure interactions. *J. Zhejiang Univ.-SCI A* **2016**, *17*, 202–214. [[CrossRef](#)]
22. Karpenko, M.; Bogdevicius, M. Investigation of hydrodynamic processes in the system—“Axial piston pumps-pipeline-fittings”. In Proceedings of the Transport Problems 2018: VII International Symposium of Young Researchers, Katowice, Poland, 25–26 June 2018; pp. 832–843.
23. Pan, Y.; Li, Y.B.; Liang, D.D. The influence of dynamic swash plate vibration on outlet flow ripple in constant power variable-displacement piston pump. *Proc. Inst. Mech. Eng. Part C-J. Mech. Eng. Sci.* **2019**, *233*, 4914–4933. [[CrossRef](#)]
24. Wang, X.; Liu, S.; Yang, L.; Wang, D. Modeling Analysis and Simulation Research of Spring-Return Plunger Pump Based on AMESim. In Proceedings of the International Conference on Cyber Security Intelligence and Analytics, CSIA 2020, Haikou, China, 28–29 February 2020; pp. 232–237.
25. Hong, H.C.; Zhao, C.X.; Zhang, B.; Bai, D.P.; Yang, H.Y. Flow Ripple Reduction of Axial-Piston Pump by Structure Optimizing of Outlet Triangular Damping Groove. *Processes* **2020**, *8*, 1664. [[CrossRef](#)]
26. Hong, H.-C.; Zhang, B.; Yu, M.; Zhong, Q.; Yang, H.-Y. Analysis and Optimization on U-shaped Damping Groove for Flow Ripple Reduction of Fixed Displacement Axial-Piston Pump. *Int. J. Fluid Mach. Syst.* **2020**, *13*, 126–135. [[CrossRef](#)]
27. Lyu, F.; Ye, S.; Zhang, J.; Xu, B.; Huang, W.; Xu, H.; Huang, X. Theoretical and Simulation Investigations on Flow Ripple Reduction of Axial Piston Pumps Using Nonuniform Distribution of Pistons. *J. Dyn. Syst. Meas. Control* **2021**, *143*, 041008. [[CrossRef](#)]
28. Deng, H.; Zhu, P.; Hu, C.; He, T. Study on Dynamic Lubrication Characteristics of the External Return Spherical Bearing Pair under Full Working Conditions. *Machines* **2022**, *10*, 107. [[CrossRef](#)]
29. Marinaro, G.; Frosina, E.; Senatore, A. A Numerical Analysis of an Innovative Flow Ripple Reduction Method for External Gear Pumps. *Energies* **2021**, *14*, 471. [[CrossRef](#)]
30. Imagine, S.A. *HYD Advanced Fluid Properties*; Technical Bulletin no. 117; Siemens: Munich, Germany, 2007.